Inhibition of CDK12 induces cancer cell dependence on activated P-TEFb via the ATM-stimulated p53 and NF-κB transcriptional programs

Zhijia Wang,[1] Caroline C. Friedel,[2] Matjaž Barborič [1,*]

[1]Department of Biochemistry and Developmental Biology, University of Helsinki, Helsinki FIN-00014, Finland

[2]Institute of Informatics, Ludwig-Maximilians-Universität München, 80333 Munich, Germany

[*]Correspondence: matjaz.barboric@helsinki.fi

ABSTRACT

P-TEFb and CDK12 facilitate transcription elongation by RNA polymerase II and play prominent roles in cancer. Understanding their functional interplay in cancer cells could inform novel therapeutic strategies. While inhibition of CDK12 downregulates unique sets of genes, which elicits genomic instability that is being exploited therapeutically, little is known about the significance of transcriptional induction in CDK12-targeted cells. We show that inhibition of CDK12 in colon cancer-derived cells activates P-TEFb and induces genes of key cancer signaling pathways, including p53 and NF-κB. As a result, cancer cells become exquisitely dependent on P-TEFb. Mechanistically, inhibition of P-TEFb ablates the induction of model genes and synergizes with CDK12 inhibitors in cancer cell elimination through activation of p53-dependent apoptosis and attenuation of NF-κB-dependent proliferation. Furthermore, we show that the DNA damage-responsive ATM kinase mediates these effects. While ATM is required for the synthetic lethality of CDK12 and P-TEFb co-targeting in p53-proficient cells, co-inhibition of ATM and CDK12 synergistically decreases viability of p53-deficient cells. Finally, pairwise targeting of CDK12, P-TEFb and transcription initiation kinase CDK7 stimulates p53-dependent apoptosis of cancer cell spheroids. We propose that the DNA damage-induced stimulation of Pol II pause release by P-TEFb at the signal-responsive genes underlies the dependence of CDK12-targeted cancer cells on P-TEFb. Together, our study provides a rationale for combinatorial targeting of CDK12 and P-TEFb or the induced oncogenic pathways in cancer.

INTRODUCTION

Transcriptional cyclin-dependent kinases (tCDKs) phosphorylate $Tyr^1Ser^2Pro^3Thr^4Ser^5Pro^6Ser^7$ heptad repeats within the C-terminal domain (CTD) of the RPB1 subunit of RNA polymerase II (Pol II) and Pol II accessory factors. This promotes transitions between discrete phases of the transcription cycle and links transcription with precursor mRNA (pre-mRNA) maturation and chromatin modification (1-3). Transcription initiation and promoter clearance is stimulated by CDK7. As a part of the ten-subunit transcription factor TFIIH, CDK7 binds Cyclin H and Mat1 and is recruited to the Pol II pre-initiation complex at gene promoters where it phosphorylates Ser5 and Ser7 residues of the Pol II CTD. At the same time, CDK7 promotes 5'-end capping of pre-mRNA and facilitates promoter-proximal pausing of Pol II by stimulating the binding of DRB-sensitivity inducing factor (DSIF) and negative elongation factor (NELF) with Pol II, which leads to its arrest in an inactive conformation (1,4). Outside of TFIIH, the trimeric CDK7-cyclin H-Mat1 complex functions as a CDK-activating kinase (CAK) for the Pol II elongation kinases positive transcription elongation factor b (P-TEFb), CDK12 and CDK13 (5). The release of Pol II from pausing is triggered by the recruitment of P-TEFb, composed of the catalytic CDK9 and a regulatory cyclin T1 or T2 subunit, which phosphorylates Ser2 residues across the CTD and its linker as well as multiple positions within both pause-inducing factors (6,7). These events convert DSIF into a positive elongation factor, lead to dissociation of NELF from Pol II, and stimulate the docking of the polymerase associated factor complex (PAFc) and SPT6 onto Pol II and the CTD linker, respectively, enabling Pol II elongation to resume (8). Subsequently, highly homologous CDK12 and CDK13 interact with cyclin K to phosphorylate the CTD at multiple positions and to stimulate processivity and elongation rate of Pol II along gene bodies by promoting the interaction of PAFc and SPT6 with elongating Pol II, which facilitates production of full-length transcripts (9-12). In keeping with their role during transcription, both P-TEFb and CDK12 regulate alternative splicing of pre-mRNA and proper transcription termination (13-17).

CDK12 has emerged as an important player in cancer. An analysis of the genetic dependency data across 1070 cancer cell lines from the Cancer Dependency Map (DepMap) project has revealed that *CDK12* is essential in close to 30% of cancer cell lines, of which average knockout effects on cell viability were similar to those of the cell-cycle oncogenes *CDK4* and *CDK6* (18). Genomic alterations of *CDK12*, which include mutations, deletions, amplifications and rearrangements, were documented in about thirty tumor types with an incidence of up to 15% of cases (19). The best understood role of CDK12 is its ability to enable genomic stability, where CDK12 promotes expression of unique sets of genes. First, CDK12 facilitates transcription elongation at long genes that function in the homologous recombination (HR) DNA repair pathway, DNA replication and cell-cycle, whereby its activity counteracts a prevalence of intronic polyadenylation sites to suppress premature pre-mRNA cleavage and polyadenylation (9,10,20,21). Second, CDK12 stimulates translation of mRNAs encoding key factors that dictate chromosome alignment and mitotic fidelity (22). Whereas disruption of these CDK12 regulatory networks likely contributes to the origin of tandem DNA duplications that are a hallmark of genomic instability in cancers with biallelic *CDK12* inactivation (21,23,24), the requirement for HR gene expression has invigorated efforts for therapeutic targeting of CDK12, particularly in combination with PARP inhibitors that are effective in HR-deficient cancer cells (25-27). As outcomes of *CDK12* alterations are context dependent, *CDK12* has been reported to function as a tumor suppressor and as an oncogene. For example, *CDK12* is a tumor suppressor in high-grade serous ovarian carcinoma, wherein its recurrent loss-of-function mutations prompt downregulation of HR genes, impairment of DNA double-strand break (DSB) repair via HR and cellular sensitivity to PARP inhibitors (28-30). Conversely, *CDK12* is co-amplified with the receptor tyrosine kinase (RTK) oncogene *HER2* (also known as *ERBB2*) in many cases of breast cancer, where it promotes migration and invasion of tumor cells by downregulation of the nuclear isoform of DNAJB6 via alternative last exon splicing (14). In addition, CDK12 can act as a facilitator or an effector of oncogenic signaling pathways. While CDK12 facilitates activation of ERBB–PI3K–AKT and WNT signaling pathways in *HER2*-positive breast cancer through promoting transcription

of an RTK adaptor IRS-1 and WNT ligands genes, respectively (31), it is constitutively activated by the hyperactive RAS–BRAF–MEK1/2–ERK1/2 signaling pathway in BRAF-mutated melanoma (32).

In contrast to CDK12, current evidence indicates that the role of P-TEFb in cancer is chiefly, if not exclusively, oncogenic. An analysis of the DepMap dataset shows that *CDK9*, just like *CDK7*, is essential for all cancer cell lines, of which knockout displays even stronger average effects than the knockout of *KRAS* or the cell-cycle *CDK4* and *CDK6* (18). Because cancer alterations of *CDK9* do not affect its expression or kinase activity in a majority of cases (33,34), many distinct mechanisms likely account for the reliance on P-TEFb. For example, genetic and epigenetic alterations in cancer cells, most notably rearrangements of *MLL1* and amplification of *MYC*, respectively, lead to redirection of P-TEFb to the oncogenes' loci, stimulating oncogenic transcription programs (35). Furthermore, P-TEFb promotes enhancer-driven transcription of *MYC* and *MCL1* oncogenes and protein stability of MYC to underwrite cancer cell dependency on these short-lived oncogenic proteins (36-38). P-TEFb also stimulates transcription of key transcription factors (TFs) of epithelial–mesenchymal transition (EMT) to promote breast cancer EMT, invasion and metastasis (39). Recently, P-TEFb has been shown to suppress mitochondria-mediated intrinsic apoptosis pathway via facilitating transcription of key genes of the oncogenic PI3K–AKT signaling cascade (40). Beyond its role in Pol II pause release, P-TEFb also promotes tumorigenesis by silencing tumor suppressor and endogenous retrovirus genes through phosphorylation of an ATP-dependent helicase BRG1 of the BAF chromatin remodeling complex, which is thought to keep this chromatin remodeler off chromatin (41).

Transcriptional activity of P-TEFb is controlled by the 7SK small nuclear ribonucleoprotein (snRNP), in which coordinated actions of the scaffolding 7SK small nuclear RNA (7SK) and three RNA-binding proteins (RBPs) inhibit the kinase. While the 7SK γ-methylphosphate capping enzyme MePCE and La-related protein 7 (LARP7) stabilize 7SK to form the tripartite core of 7SK snRNP, HEXIM1 interacts with 7SK of the core to bind and inhibit P-TEFb (42,43). As 7SK snRNP contains a major fraction of cellular P-TEFb, it acts as a molecular reservoir from which active P-TEFb can be deployed in a prompt and regulated manner to accommodate cellular transcriptional needs in unison with stimuli-specific transcription factors that recruit the released P-TEFb to promote target gene activation. Indeed, a host of perturbations and stimuli, including transcriptional blockade, genotoxic stress, viral infection and cell growth, trigger activation of P-TEFb, whereby numerous 7SK-binding factors have been proposed to release P-TEFb enzymatically and/or allosterically via a large-scale conformational switching of 7SK (43,44).

While CDK12-dependent transcription has been explored extensively and harnessed in therapeutic settings, little attention has been given to genes that are induced upon the inhibition of CDK12. In principle, the induced genes could elicit novel vulnerabilities and/or resistance mechanisms of CDK12-targeted cancer cells. Intriguingly, transcriptional responses to CDK12 inhibition and ultraviolet (UV) irradiation resemble each other in that they both show a gene length-dependent Pol II elongation effect, wherein transcription of short genes is induced or remains unaltered, whereas increasingly long genes become progressively repressed (10,45,46). Importantly, while CDK12 perturbation increases DNA damage (9,25,26,29,30), the release of P-TEFb from 7SK snRNP is a hallmark of cellular DNA damage response (DDR), whereby activated P-TEFb shapes a transcriptional response enabling survival of stressed cells (47,48). In this study, we investigated whether inhibition of CDK12 induces genes through activation of P-TEFb. Furthermore, we explored the nature and functional significance of the induced transcriptome. Our results show that inhibition of CDK12 stimulates P-TEFb and important cancer signaling pathways, which renders cancer cells highly sensitive to P-TEFb inhibitors. Hence, our study provides a rationale for elimination of cancer cells by co-targeting the principal kinases that stimulate transcription elongation by Pol II.

MATERIALS AND METHODS

Reagents

A list of reagents used in the study is provided in Supplementary Table S1.

Cell lines

HCT116 cell line and its derivatives were cultured in McCoy's 5A Medium (Merck) supplemented with 10% FBS and 100 U/ml penicillin/streptomycin. CCD 841 CoN cell line was cultured in Eagle's Minimum Essential Medium (Lonza) supplemented with 10% FBS and 100 U/ml penicillin/streptomycin. All cell lines were maintained at 37°C with 5% CO_2. Cell lines were confirmed regularly to be mycoplasma-free using a qPCR-based Mycoplasmacheck detection kit (Eurofins). Cell lines were not authenticated by us, but retrieved from trusted sources as listed in Supplementary Table S1D.

Chemicals

NVP-2, THZ531 and MLN120B were from MedChemExpress. THZ532 and YLK-5-124 were a gift from Nathanael S. Gray's Laboratory (Stanford University, USA). iCDK9 was a gift from Qiang Zhou's Laboratory (University of California, Berkley, USA). 3-MB-PP1 was from Cayman Chemical. KU-60019 was from Selleck Chemicals. TNF-α was from Proteintech. For more information on the chemicals, see Supplementary Table S1B.

Co-immunoprecipitation Assay

HCT116 and HCT116 *CDK12* $^{as/as}$ cells grown on 60 mm plates were treated as indicated at 90 % confluency, after which whole-cell extracts were prepared using 800 µl of lysis buffer C (20 mM Tris-HCl, 0.5% NP-40, 150 mM NaCl, 1.5 mM MgCl2, 10 mM KCl, 10% Glycerol, 0.5 mM EDTA, pH 7.9) on ice for 1 h in the presence of EDTA-free Protease Inhibitor Cocktail (Merck) and cleared by centrifugation at 20,000 g for 15 min. Buffer C-equilibrated Dynabeads Protein G (Thermo Fisher Scientific) were incubated with 1 µg of the anti-HEXIM1 antibody (Everest Biotech) for 2 hr at 4 °C and washed three times with the lysis buffer prior to incubation with 800 µl of the whole-cell extracts overnight at 4 °C. The beads were washed three times with the lysis buffer and boiled in SDS loading buffer supplied with 10% of β-Mercaptoethanol for 5 min. Proteins were separated using SDS-PAGE, transferred to nitrocellulose membrane and analyzed by Western blotting. Thirty µl of the whole-cell extract was used as a loading control.

Western Blotting Assay and Antibodies

Whole-cell extracts were prepared using lysis buffer C (20 mM Tris-HCl, 0.5% NP-40, 150 mM NaCl, 1.5 mM MgCl2, 10 mM KCl, 10% Glycerol, 0.5 mM EDTA, pH 7.9) on ice for 1 h in the presence of EDTA-free Protease Inhibitor Cocktail (Merck). Lysates were cleared by centrifugation at 20,000 g for 15 min, boiled in SDS loading buffer supplied with 10% of β-Mercaptoethanol for 5 min, separated using SDS-PAGE, transferred to nitrocellulose membrane and analyzed by Western blotting. The following antibodies were used according to manufacturers' instructions: anti-CDK9 (Santa Cruz Biotechnology, 1:4000); anti-p53 (Santa Cruz Biotechnology, 1:3000); anti-p21 (Santa Cruz Biotechnology, 1:4000); anti-GAPDH (Santa Cruz Biotechnology, 1:10,000); anti-HEXIM1 (Everest Biotech, 1:000); anti-CDK12 (Cell Signaling Technology, 1:1000); anti-CDK7 (Cell Signaling Technology, 1:1000). Manufacturers provide validation for all antibodies. For more information on the antibodies, see Supplementary Table S1A.

Target Engagement Assay

HCT116 cells were treated with the indicated concentrations of THZ531 or DMSO for the indicated time. Whole-cell extracts were prepared using NP-40 lysis buffer (Thermo Fisher Scientific) supplemented with complete protease inhibitor cocktail (Merck), PhosSTOP phosphatase inhibitor cocktail (Merck) and 1 mM of Phenylmethanesulfonyl fluoride (Merck). The extracts containing 1 mg of total protein were first incubated with 1 µM of biotin-THZ1 at 4 °C overnight, after which the complexes were affinity purified using 30 µl of streptavidin agarose beads for 2 h at 4 °C. The beads were washed three times with the lysis buffer and boiled for 10 min in SDS loading buffer. The proteins were separated using SDS-PAGE and analyzed by Western blotting. Fifty micrograms of total protein was used as a loading control.

RNA Extraction and RT-qPCR Assay

HCT116 cells were seeded on 6-well plates for 16 h and treated at 80% confluency with the indicated compound combinations and corresponding volume of DMSO. RNA samples were extracted using TRI Reagent (Merck), DNase-treated with the Turbo DNA-Free kit (Thermo Fisher Scientific), and reverse transcribed with M-MLV reverse transcriptase (Thermo Fisher Scientific) and random hexamers (Thermo Fisher Scientific) according to the manufacturers' instructions. qPCR reactions were performed with diluted cDNAs, primer pairs that spanned exon-intron junctions, and FastStart Universal SYBR Green QPCR Master (Rox) (Sigma) using Roche LightCycler 480. Primers were from Integrated DNA Technologies and designed using PrimerQuest Tool. Results from three independent experiments were normalized to the values of *GAPDH* mRNA and DMSO-treated cells, and plotted as the mean ± s.e.m. Sequences of the primers are listed in Supplementary Table 1F.

Cytotoxicity, Viability and Apoptosis Assays

Cytotoxicity, viability, and apoptosis assays were conducted using CellTox Green Cytotoxicity Assay (Promega), CellTiter-Glo 2.0 Cell Viability Assay (Promega) and RealTime-Glo Annexin V Apoptosis and Necrosis Assay (Promega), respectively, according to manufacturer's instructions. For cytotoxicity and apoptosis assays, HCT116 cells were seeded at density of 20,000 cells/well on 96-well plates for 16 h prior to the treatments, while for the seven-day viability assays, HCT116 cells were seeded at density of 5,000 cells/well on 12-well plates for 16 h prior to the treatments. Fluorescence and luminescence measurements were taken at the indicated time points using PerkinElmer Victor X3 reader. Results from at least three independent experiments are presented as values relative to the values of DMSO-treated cells and plotted as the mean ± s.e.m.

Spheroid Apoptosis Assay

HCT116 cells were seeded at density of 400 cells/well on Nunclon Sphera 96-well U-bottom ultra low attachment 3D cell culture plate (Thermo Fisher Scientific) and spun down at 200 g for 10 minutes. After culturing the cells for 48 h to allow for spheroid formation, the spheroids were treated with the indicated compounds over the subsequent 48 h period. Apoptosis assay was conducted using RealTime-Glo Annexin V Apoptosis and Necrosis Assay (Promega) according to manufacturer's instructions. Luminescence measurements were taken at the indicated time points using PerkinElmer Victor X3 reader. Results from at least three independent experiments are presented as values relative to the values of DMSO-treated cells and plotted as the mean ± s.e.m.

Analysis of RNA Sequencing Datasets

Gene expression changes in nuclear RNA obtained from HCT116 *CDK12* $^{as/as}$ cell line treated with 3-MB-PP1 for 4.5 h were taken from the study of Manavalan *et al.* (Dataset EV2) (21). The RNA-seq data are available at the Gene Expression Omnibus (GEO) repository (NCBI) under the accession code GEO: GSE120071. Gene expression changes obtained from HCT116 cells treated with NVP-2 for 8 h were taken from the study of Wang *et al.* (40). The RNA-seq are available at the Gene

Expression Omnibus (GEO) repository (NCBI) under the accession code GEO: GSE216610. TT-seq expression changes obtained from IMR-32 cells treated with THZ531 for 2 h were taken from the study of Krajewska *et al.* (Supplementary Data 2) (10). The TT-seq data are available at the Gene Expression Omnibus (GEO) repository (NCBI) under the accession code GEO: GSE113313. Changes of metabolically-labeled RNAs obtained from Hela cells treated with 4-NQO for 2 h were taken from the study of Bugai *et al.* (47) The 4sU-seq data are available at the Gene Expression Omnibus (GEO) repository (NCBI) under the accession code GEO: GSE110272. Genes were considered significantly regulated if the multiple testing adjusted *P*-value by the Benjamini and Hochberg method (49) was ≤ 0.001, up-regulated with a log2 fold-change ≥ 1 and down-regulated with a log2 fold-change ≤ -1. NVP-2 sensitive genes were defined as genes significantly down-regulated by NVP-2 treatment (adj. *P*-value was ≤ 0.001, log2 fold-change ≤ -1). Volcano plots show log2 fold-changes on the x-axis and log10 (adjusted p-value) on the y-axis. Gene lengths were obtained from Ensembl. Distribution of gene lengths for up- and down-regulated genes is shown as boxplots. Boxes represent the range between the first and third quartiles for each condition. Gray horizontal lines in boxes show the median. The ends of the whiskers (vertical lines) extend the box by 1.5 times the inter-quartile range. Data points outside this range (outliers) are shown as small circles. Volcano plots and boxplots were created in R (https://www.R-project.org/). Gene set enrichment analysis on log2 fold-changes for protein-coding genes was performed using the command line tool from http://www.gsea-msigdb.org/ (version 4.0.2) (50) and hallmark gene sets from Molecular Signatures Database.

Cell-cycle analysis

HCT116 cells were seeded on 60 mm dishes and cultured to approximately 70% confluence. The cells were synchronized by serum deprivation for 24 h prior to their culture in the serum-containing medium for 24 h in the presence of DMSO (-), THZ531 (50 nM) and NVP-2 (50 nM). After trypsinization, cell pellets were collected, washed with PBS and fixed by ice-cold 70% ethanol. For FACS analysis, the cells were washed in PBS and incubated overnight at 4°C in freshly prepared staining solution in PBS containing 50 g/ml propidium iodide, 0.1% Triton X-100 and 0.2 mg/ml DNase-free Rnase A. FACS was performed by BD Accuri C6 and data was analysed by FlowJo.

Quantification and Statistical Analysis

P-values of gene expression changes were corrected by multiple testing using the method by Benjamini and Hochberg (49) for adjusting the false discovery rate (FDR) and an adjusted *P*-value cutoff of 0.001 was applied. Data shown for all RT-qPCR experiments and functional assays were collected from three biological replicates as indicated in individual figure legends and are presented as means ± s.e.m. Statistical significance and *P*-values were determined by Student's *t* test performed between the indicated paired groups of biological replicates. Where the results were not statistically significant, *P*-values are not indicated.

RESULTS

Inhibition of CDK12 stimulates the release of P-TEFb from 7SK snRNP

Considering that perturbation of CDK12 results in DNA damage (9,25,26,29,30) and that genotoxic stress triggers activation of P-TEFb to enable a pro-survival transcriptional response (47,48), we hypothesized that selective inhibition of CDK12 activates P-TEFb (Figure 1A). To test this prediction, we performed co-immunoprecipitation (co-IP) assays to monitor the interaction of endogenous CDK9 with its inhibitory protein HEXIM1 in whole cell extracts of cells that were treated or not with inhibitors of CDK12. We conducted these experiments using HCT116 cells, a well-established model of colorectal cancer encoding the oncogenic KRAS ^{G13D} and PIK3CA ^{H1047R} proteins. We first inhibited CDK12 with THZ531, a potent and selective molecular probe which covalently modifies the cysteine residue 1039 positioned outside of the conserved kinase domain (51). Treatment of HCT116 cells with 300 or 400 nM of THZ531 resulted in a time-dependent dissociation of CDK9 from HEXIM1, indicative of P-TEFb activation (Figure 1B). In contrast, 400 nM of THZ532, the enantiomer of THZ531 with a diminished ability to inhibit CDK12 (51), failed to do so. Concurrently, both concentrations of THZ531 but not 400 nM of THZ532 led to a time- and dose-dependent decrease in mRNA levels of *BRCA1* and *FANCD2*, the established CDK12-dependent genes of the HR pathway (9,29), providing evidence that the THZ531 treatments inhibited CDK12 in our system (Supplementary Figure S1A).

In comparison to CDK12, THZ531 displays more than 50-fold lower activity towards CDK7 and CDK9 in fixed-endpoint *in vitro* kinase assays (51). We nevertheless assessed whether THZ531 retained specificity towards CDK12 during the above co-IP experiments. We used a biotin-modified version of THZ1, a covalent inhibitor of CDK7 and a precursor to THZ531 that interacts with both CDK7 and CDK12 (51,52), to affinity purify both kinases from HCT116 cell extracts and investigated whether THZ531 prevents CDK12 but not CDK7 from binding biotinylated THZ1. Indeed, treatment of HCT116 cells with 300 nM or 400 nM of THZ531 countered the affinity purification of CDK12 in time-dependent manner, while CDK7 remained bound to biotinylated THZ1 across all conditions tested (Figure 1C). These results demonstrated that both concentrations of THZ531 that activated P-TEFb targeted CDK12 specifically over CDK7.

However, the only known kinase that is in addition to CDK12 inhibited by THZ531 at a comparable potency is its highly homologous counterpart CDK13 (51), which is not involved in facilitating DNA repair (9,53). To demonstrate that inhibition of CDK12 alone provokes the release of CDK9 from HEXIM1, we took a chemical genetic approach. We conducted co-IP assays in HCT116 *CDK12* $^{as/as}$ cell line in which both alleles of *CDK12* were replaced with *CDK12* ^{F813G}, generating analog-sensitive version of CDK12 (asCDK12) that is specifically inhibited by treatment of these cells with bulky adenine analogs such as 3-MB-PP1 (21). Recapitulating the results with THZ531, treatment of HCT116 *CDK12* $^{as/as}$ cell line with 3-MB-PP1 perturbed the interaction of CDK9 with HEXIM1 (Figure 1D). In contrast, we did not observe this effect in the parental HCT116 cell line which is refractory to the inhibition of CDK12 by 3-MB-PP1 (Figure 1D). Confirming that 3-MB-PP1 specifically inhibited asCDK12, 3-MB-PP1 treatment decreased mRNA levels of *BRCA1* and *FANCD2* in HCT116 *CDK12* $^{as/as}$ cells but not in the parental counterpart (Supplementary Figure S1B). Together, we conclude that inhibition of CDK12 activates P-TEFb by triggering its release from 7SK snRNP.

Inhibition of CDK12 induces genes of key cancer signaling pathways through ATM and P-TEFb

Previous reports have established that inhibition of CDK12 leads to down-regulation as well as induction of genes (12,15,21). However, in contrast to the down-regulated genes (9,10,20,21), little is known about the nature of the induced genes and the mechanisms governing this induction. In light of our findings above, we postulated that activation of P-TEFb facilitates gene induction when

CDK12 is inhibited. To this end, we first re-analyzed gene expression fold-changes of nuclear RNA sequencing (RNA-seq) data from synchronized HCT116 *CDK12* $^{as/as}$ cells treated for 4.5 h with DMSO or 3-MB-PP1 (21). Applying our criteria (p-adj ≤ 0.001; log2 fold-change ≥ 1), we identified 12.32% differentially expressed protein-coding genes (n = 12,495). Of these, 1235 genes were down-regulated while 304 were induced (Figure 2A). Consistent with previous studies on transcriptional response to CDK12 inhibition and genotoxic stress (10,46,47,54), the induced genes were considerably shorter than the repressed genes (Figure 2B). To estimate the role of P-TEFb in the gene induction, we utilized our published differential gene expression data from HCT116 cells treated for eight hours with DMSO or NVP-2 (40), which is a highly selective inhibitor of P-TEFb that effectuates potent anti-cancer activity at non-toxic doses (55,56). Out of the 205 3-MB-PP1-induced genes which are present in the data set of differentially expressed genes upon NVP-2 treatment, two thirds of them show at least 20% reduction of their basal expression levels in NVP-2-treated cells (Supplementary Figure S2A). These findings suggest a prominent role of activated P-TEFb in the transcriptional induction elicited by inhibition of CDK12.

To gain an insight into the nature of genes induced by CDK12 inhibition with 3-MB-PP1, we conducted gene set enrichment analysis (GSEA) of the differentially expressed genes using the hallmark gene set collection of the Molecular Signatures Database (50,57). The analysis revealed that the top five gene sets enriched amongst the induced genes represented crucial oncogenic pathways, including NF-κB, hypoxia and MYC (Figure 2C and Supplementary Table S2A). In addition, the genes of the tumor suppressive p53 pathway and those induced in response to ultraviolet (UV) irradiation featured prominently, supporting previous work that showed accumulation of p53 and increased DNA damage upon genetic or pharmacological perturbation of CDK12 (9,20,26). Corroborating this analysis, these gene sets were also enriched within the induced genes of the metabolically-labeled transcriptome of a *MYCN*-amplified neuroblastoma cell line IMR-32 treated with THZ531 and cervical cancer-derived HeLa cells exposed to the DNA-damaging UV mimetic 4-nitroquinoline 1-oxide (4-NQO) (10,47) (Figure 2C and Supplementary Table S2B, C). Thus, the observed transcriptional response to CDK12 inhibition is not cell line-specific and bears similarity to the one elicited by genotoxic stress.

To validate these analyses and to address the role of P-TEFb in gene induction following CDK12 inhibition, we quantified precursor mRNA (pre-mRNA) levels of the pro-survival *FOS* and *CDKN1A* model genes with RT-qPCR. While both of these genes, which encode the c-Fos subunit of the oncogenic transcription factor AP-1 and the CDK inhibitor p21, belong to the hallmark NF-κB, p53 and hypoxia pathway gene sets, *FOS* is a member of the set induced by UV (57). Furthermore, genotoxic stress elicited by 4-NQO increases transcription of *FOS* and *CDKN1A* in a P-TEFb-dependent manner (47). In line with our transcriptome analyses and the kinetics of the release of CDK9 from HEXIM1, treatment of HCT116 cells with 300 or 400 nM of THZ531 led to a time-dependent induction of *JUN* and *CDKN1A*, whereas 400 nM of THZ532 failed to do so (Supplementary Figure S2B). Importantly, the induced levels of freshly produced transcripts of both genes were blunted by the addition of NVP-2 (Figure 2D). We confirmed these results by selective inhibition of CDK12 with 3-MB-PP1 in HCT116 *CDK12* $^{as/as}$ cells, wherein both genes were induced in a P-TEFb-dependent manner (Figure 2E). Predictably, none of this occurred in the parental HCT116 cells (Figure 2E).

Given that perturbation of CDK12 induces DSBs (25,29,30), we next asked whether the ataxia-telangiectasia mutated (ATM) protein kinase played a role in the transcriptional induction of *FOS* and *CDKN1A* in CDK12-inhibited cells. ATM is a chief orchestrator of the cellular DDR. DNA lesions, most notably DSBs, activate ATM, prompting phosphorylation of a wide range of downstream targets that regulate DNA repair, cell-cycle checkpoints, and apoptosis (58). Importantly, ATM has been linked to the enriched hallmark pathways in CDK12-targeted cells identified above. While hypoxia and overexpression of MYC activate ATM (59,60), the kinase induces NF-κB and p53 pathways as well as hypoxic response in part by phosphorylation of NF-κB, p53 and hypoxia-inducible HIF1A, which in turn stimulate signal-induced gene transcription networks (59,61-63). Indeed, the highly

selective ATM inhibitor KU-60019 (64) interfered with the induction of *FOS* and *CDKN1A* by THZ531 (Figure 2F).

Finally, we conducted immunoblotting analysis to confirm that inhibition of CDK12 increases the expression of *CDKN1A* in manner that depends on P-TEFb and ATM. As *CDKN1A* represents a classical p53 target gene, we performed this experiment also in an isogenic *TP53* $^{-/-}$ derivative of HCT116 cells, in which *TP53* was inactivated by disrupting exon 2 of both alleles (65). In line with the transcript analyses, inhibition of CDK12 by THZ531 increased the levels of p21 in a P-TEFb-, p53- and ATM-dependent manner (Figure 2G, H). Importantly, inhibition of CDK12 prompted the accumulation of p53 (Figure 2G, H), corroborating the enrichment of the hallmark p53 pathway gene set within the induced genes. Together, we conclude that activation of P-TEFb facilitates the induction of a subset of genes elicited by the inhibition of CDK12, wherein ATM plays a key role.

Inhibition of CDK12 increases the dependency of cancer cells on P-TEFb

Given our findings gathered thus far and a growing body of work on the pro-survival role of P-TEFb in cancer, we next hypothesized that selective targeting of CDK12 renders cancer cells dependent on P-TEFb. As the hallmark p53 pathway gets activated in CDK12-inhibited cells, we further postulated that the status of p53 could play a key role in this process. We therefore measured cellular response to selective CDK12 and P-TEFb inhibitors by utilizing the parental and TP53 $^{-/-}$ HCT116 cell lines.

We first used fluorescence-based cytotoxicity assay, in which compromised membrane integrity of dead cells is proportional to fluorescence signal generated by the binding of an otherwise cell impermeable cyanine dye to DNA. As predicted, we found that inhibition of CDK12 by THZ531 sensitized HCT116 cells to P-TEFb inhibitors NVP-2 and iCDK9 (Figure 3A and Supplementary Figure S3A). In contrast, cytotoxic response to the co-targeting was largely diminished in the absence of p53 (Figure 3A), indicating that cancer cells become markedly dependent on P-TEFb upon activation of the p53-driven transcriptional program. In accordance with the key role of ATM in the activation of p53 (62), pharmacological inhibition of ATM by KU-60019 blunted the dependency of CDK12-inhibited HCT116 cells on P-TEFb (Figure 3B). Importantly, cytotoxicity elicited by the concurrent inhibition of CDK12 and P-TEFb was specific to cancer cells as co-treatment of THZ531 and NVP-2 did not impact a non-transformed colorectal epithelial cell line CCD 841 CoN (Figure 3C). Confirming our results with THZ531, we found that selective inhibition of CDK12 with 3-MB-PP1 in HCT116 *CDK12* $^{as/as}$ cells augmented cytotoxicity elicited by NVP-2 or iCDK9, whereas this effect was absent in the parental HCT116 cells (Figure 3D and Supplementary Figure S3B).

To provide complementary evidence for the observed synthetic lethality of CDK12 and P-TEFb co-targeting, we next used the above cell lines and monitored their viability for up to seven days with a luminescence-based assay in which the number of metabolically active cells is determined by quantifying the levels of ATP via luciferase reaction. While chronic treatment of HCT116 cells with THZ531, NVP-2 and iCDK9 alone affected them similarly to the DMSO control, concurrent inhibition of CDK12 and P-TEFb resulted in a synergistic drop in cell viability, which was particularly profound when we used iCDK9 to inhibit P-TEFb (Figure 3E and Supplementary Figure S3C, left). Surprisingly, this effect was independent of p53 (Figure 3E and Supplementary Figure S3C, right), suggesting that activation of an additional pathway elicited by CDK12 inhibition can also augment cellular dependency on P-TEFb. We corroborated these results using the asCDK12 system, in which co-administration of 3-MB-PP1 and NVP-2 or iCDK9 decreased viability of HCT116 *CDK12* $^{as/as}$ but not the parental cells (Figure 3F and Supplementary Figure S3D). Together, we conclude that selective inhibition of CDK12 renders HCT116 cells highly dependent on P-TEFb. Furthermore, cytotoxicity elicited by the combination treatment depends on the ATM-p53 axis.

Co-targeting of CDK12 and P-TEFb stimulates cancer cell death by p53-dependent apoptosis

We next investigated further the significance of the hallmark p53 pathway for the heightened reliance of HCT116 cells on P-TEFb following selective inhibition of CDK12. Upon activation, the DNA-binding p53 orchestrates diverse tumor-suppressive transcriptional programs, amongst which cell-cycle arrest and apoptosis are best-defined (66). Hence, we conducted cell-cycle and apoptosis assays in the absence or presence of selective inhibitors of CDK12 and P-TEFb. Given the clear-cut ability of p53 to enable cytotoxicity in response to CDK12 and P-TEFb co-targeting (Figure 3 and Supplementary Figure S3), we postulated that stimulation of p53-dependent apoptosis is the culprit. To quantify apoptosis, we utilized a luminescence-based assay that measures apoptosis-induced exposure of phosphatidylserine on the outer surface of cell membrane through time. The assay uses two Annexin V fusion proteins each containing a fragment of NanoBit Luciferase, of which complementation is achieved upon binding of Annexin V with phosphatidylserine (67). In concordance with the above cytotoxicity and viability data, THZ531 or NVP-2 treatment of HCT116 cells alone elicited a defect in the G1/S phase transition of the cell-cycle and low levels of apoptosis (Figure 4A, B). On the contrary, we detected robust apoptosis of cells exposed to the combination treatment, which depended on p53 and started to become apparent at about twelve hours into the treatment (Figure 4B). Likewise, we observed the same phenotype when we targeted P-TEFb with iCDK9 in place of NVP-2 (Supplementary Figure S4A).

To validate the apoptosis findings in a physiologically more relevant setting, we next assessed whether co-inhibition of CDK12 and P-TEFb stimulates apoptotic death of HCT116 spheroids. Namely, spheroid cultures have emerged as a viable pre-clinical platform for evaluating anti-cancer treatments (68). Unlike monolayer cultures, spheroids possess several *in vivo* hallmarks of tumor microenvironments such as spatial architecture of cells with different proliferation status, complex cell-cell contacts, oxygen and nutrient gradients, and rewired metabolism. As reported in our previous study (40), we established scaffold-free spheroids of about 400 μm in size before treating them for two days with DMSO, THZ531, NVP-2 or iCDK9 alone and in combination, during which we monitored kinetics of apoptosis utilizing the quantitative Annexin V assay. We observed that THZ531, NVP-2 and iCDK9 treatments in isolation elicited HCT116 spheroid apoptosis at vanishingly low levels that were indistinguishable from the DMSO control. In contrast, the co-targeting of CDK12 and P-TEFb elicited robust apoptosis in a highly synergistic manner (Figure 4C and Supplementary Figure S4B, left). As anticipated, the combination treatments failed to result in apoptosis of *TP53* null spheroids (Figure 4C and Supplementary Figure S4B, right). Likewise, 3-MB-PP1 treatment sensitized HCT116 *CDK12* $^{as/as}$ but not the parental HCT116 spheroids to P-TEFb inhibitors NVP-2 and iCDK9 (Figure 4D and Supplementary Figure S4C). Together, we conclude that inhibition of CDK12 primes cancer cells for p53-dependent apoptosis, which is triggered in a synergistic manner by co-inhibition of P-TEFb.

Inhibition of CDK12 renders cancer cells dependent on the NF-κB signaling pathway

Given that co-inhibition of CDK12 and P-TEFb decreased the viability of HCT116 cells independently of p53, we reasoned that the targeting of CDK12 exposed novel vulnerabilities of cancer cells that could be exploited. To address this possibility, we turned our attention to the oncogenic pathways that were enriched within the genes induced by the inhibition of CDK12 (Figure 2C and Supplementary Table S2A, B). We focused on the top-ranked NF-kB signaling pathway stimulated by TNF-α, which has emerged as a potential target in cancer. This canonical NF-kB pathway promotes genesis and progression of cancer by facilitating proliferation, survival, inflammation, angiogenesis and invasion of tumor cells, and plays a role in the development of resistance to chemotherapy (69). In fact, the NF-kB pathway was the second most enriched pathway in tumors with hypertranscription, a recently revealed hallmark of aggressive human cancers (70). Importantly, NF-kB pathway can be stimulated from the nucleus by the DNA damage-induced activation of ATM (61). In both modes of the pathway activation, the key event is the signal-induced phosphorylation of the inhibitor of κB (IκB) by the IκB kinase β (IKKβ), which alleviates the cytoplasmic retention of

NF-κB through IκB degradation, prompting stimulation of NF-κB-dependent proliferative and anti-apoptotic gene transcription program (Figure 5A).

To determine contribution of this pathway to the synthetic lethality of CDK12 and P-TEFb co-targeting, we first asked whether its direct activation by TNF-α heightens the dependency of HCT116 cells on P-TEFb. Mirroring our findings with CDK12 inhibition, cytotoxicity assays revealed that TNF-α treatment sensitized HCT116 cells to P-TEFb inhibitors NVP-2 and iCDK9 in a p53-dependent manner (Figure 5B and Supplementary Figure S5A). Correspondingly, kinetic apoptosis measurements of the parental and *TP53* null HCT116 cell spheroids exposed to TNF-α and NVP-2 showed that unlike the individual treatments, the combination treatment elicited apoptosis in a highly synergistic and largely p53-dependent fashion (Figure 5C). Furthermore, while the chronic treatment of both HCT116 cell lines with TNF-α and NVP-2 alone decreased cell viability only modestly, the combination treatment led to a synergistic drop that did not depend on p53 (Figure 5D). Thus, activation of the NF-kB pathway alone renders the viability of cancer cells sensitive to P-TEFb inhibition in a p53-independent manner.

We next probed the functional significance of the NF-kB pathway for gene induction and cell viability in CDK12-targeted HCT116 cells. To inhibit activation of the NF-kB pathway, we first utilized MLN120B, the selective, ATP-competitive inhibitor of IKKβ (71). Indeed, addition of MLN120B lowered the induction of *FOS* and *CDKN1A* model genes upon THZ531 and 3-MB-PP1 treatment of the parental and HCT116 *CDK12* $^{as/as}$ cells, respectively (Figure 5E, F). Correspondingly, THZ531-induced increase in the levels of p21 was blunted in the presence of MLN120B (Figure 5G). Critically, while the inhibition of CDK12 and IKKβ alone by THZ531 and MLN120B, respectively, affected viability of the parental and *TP53* null HCT116 cells only slightly, the co-targeting decreased it in a synergistic and p53-independent fashion (Figure 5H). Likewise, co-administration of 3-MB-PP1 and MLN120B synergized in lowering viability of HCT116 *CDK12* $^{as/as}$ but not the parental cells (Figure 5I). Importantly, blockade of the DNA damage-induced NF-kB signaling pathway with the ATM inhibitor KU-60019 led to a dramatic reduction in the viability of THZ531-treated parental and *TP53* null HCT116 cells (Figure 5J). Together, we conclude that selective inhibition of CDK12 renders HCT116 cells highly dependent on the oncogenic NF-kB pathway irrespectively of the status of *TP53*.

Inhibition of CDK12 or P-TEFb switches the fate of CDK7-inhibited cancer cells from cell-cycle arrest to apoptosis

That co-targeting of CDK12 and P-TEFb decreased viability of HCT116 cells prompted us to assess whether targeting of these critical transcriptional kinases in combination with CDK7 also yields the same phenotype. Apart from controlling gene transcription, cytoplasmic CDK7 is a master facilitator of cell-cycle progression by acting as a CAK for key cell-cycle CDKs, including CDK1, 2, and 4 (72). Hence, CDK7 represents an appealing target in cancer.

Not surprisingly, selective inhibition of CDK7 in various cell lines or in the analog-sensitive HCT116 *CDK7* $^{as/as}$ setting results in cell-cycle arrest at the G1/S transition, in part by attenuation of the E2F-driven gene expression program (73,74). As elimination of cancer cell by irreversible cell death is a desirable outcome of any effective cancer treatment (75,76), we examined whether the targeting of CDK12 or P-TEFb switches the fate of CDK7-inhibited cells from cell-cycle arrest to apoptosis. To inhibit CDK7, we employed YKL-5-124, a nanomolar covalent inhibitor that targets cysteine 312 on CDK7 and shows over 100-fold greater selectivity for CDK7 over P-TEFb and CDK2 (74). In agreement with earlier reports (73,74), treatment of the parental and *TP53* null HCT116 cells with YKL-5-124 was not cytotoxic. However, co-administration of THZ531 or NVP-2 sensitized HCT116 cells to CDK7 inhibition in a p53-dependent manner (Figure 6A, B). That p53 enables the death of CDK7 and CDK12 co-targeted cells is consistent with a previous report demonstrating that activation of the p53 transcriptional program sensitized cancer cells to CDK7 inhibitors (77).

Importantly, the combination treatments failed to affect the non-transformed CCD 841 CoN cells (Supplementary Figure S6A, B). Corroborating these results, selective inhibition of CDK12 by 3-MB-PP1 in HCT116 *CDK12* $^{as/as}$ cells and P-TEFb by iCDK9 in HCT116 cells was toxic in combination with CDK7 inhibition by YKL-5-124 (Supplementary Figure S6C, D).

To extend these findings, we conducted viability assays using the parental and *TP53* null HCT116 cells. Whereas chronic treatment of HCT116 cells with the three tCDK inhibitors alone had a minimal effect on cell viability, co-administration of YKL-5-124 with THZ531 or NVP-2 led to a substantial and synergistic decrease of cell viability that did not require p53 (Figure 6C, D). These results support the above cytotoxicity findings and mirror the detrimental effect of CDK12 and P-TEFb co-targeting on cell viability.

Finally, we monitored apoptosis of the parental and *TP53* null HCT116 cell spheroids treated with the tCDK inhibitors in isolation or combination for 48 hours. While treatment of the spheroids with YKL-5-124, THZ531 and NVP-2 alone stimulated apoptosis similarly to the DMSO control, co-administration of YKL-5-124 with THZ531 or NVP-2 elicited apoptosis in a highly synergistic and p53-dependent fashion (Figure 6E, F). Corroborating these findings, 3-MB-PP1 treatment sensitized HCT116 *CDK12* $^{as/as}$ but not the parental HCT116 spheroids to inhibition of CDK7 by YKL-5-124 (Supplementary Figure 6E). Likewise, co-targeting of CDK7 and P-TEFb by YKL-5-124 and iCDK9 led to a synergistic and p53-dependent stimulation of apoptosis (Supplementary Figure S6F). Collectively, these results confirm findings of the CDK-cyclin genetic co-dependencies of the DepMap project, where amongst cyclin genes, *CCNH* encoding the cyclin H of CDK7 is the top co-dependency of *CDK12*, whereas *CCNT1* encoding the cyclin T1 partner of CDK9 is the runner up co-dependency of CDK7 (18). Furthermore, they are in agreement with impressive anti-cancer activity of THZ1 in multiple in vivo models (52,78,79), wherein this precursor to THZ531 co-inhibits CDK7 alongside CDK12/13 (51). Together, we conclude that selective inhibition of CDK12 or P-TEFb switches the fate of CDK7-inhibited HCT116 cells from cell-cycle arrest to apoptosis.

DISCUSSION

An increasingly appreciated significance of tCDKs and deregulated transcription for cancer biology has put the prospects of therapeutic targeting of tCDKs into the spotlight. In this study, we selectively inhibited CDK12 by pharmacological and chemical genetic means in a well-established cell line model of colorectal cancer to uncover mechanistic and functional aspects of the induced transcriptome. We found that inhibition of CDK12 activated P-TEFb and induced genes of prominent tumor suppressive and oncogenic signaling pathways exemplified by p53 and NF-κB, respectively. In turn, the CDK12-targeted cancer cells became highly sensitive to selective inhibitors of P-TEFb, which interfered with the gene induction and led to a synergistic elimination of cancer cells by ATM-mediated stimulation of p53-dependent apoptosis and attenuation of NF-κB-dependent cell proliferation. Finally, the pairwise inhibition of CDK12, P-TEFb and CDK7 stimulated apoptosis of cancer cell spheroids. Therefore, we provide a rationale for combinatorial targeting of CDK12 and P-TEFb or oncogenic signaling pathways in cancer.

Our study reveals a mechanism that governs the induced gene expression programs in CDK12-targeted cells. We demonstrate that inhibition of CDK12 provokes activation of P-TEFb through its release from the inhibitory 7SK snRNP reservoir, whereby most of the kinase leaves the complex within an hour of CDK12 inhibition. This finding is reminiscent of the release of P-TEFb from 7SK snRNP following an acute degradation of the MED14 subunit of the Mediator complex, which augmented the rate of Pol II pause release genome-wide to restore transcription at most genes (80). The kinetics of P-TEFb activation provides an explanation for the progressive increase of the bulk of CTD Ser2 phosphorylation levels that was observed within six hours of inhibiting asCDK12 with 3-MB-PP1 (21). Our analyses of model genes and RNA-seq experiments in which we employed the selective P-TEFb inhibitor NVP-2 suggest a prominent role of the activated P-TEFb in the gene induction upon CDK12 inhibition. Indeed, prior work using THZ531-treated neuroblastoma cells showed a rapid and bidirectional accumulation of metabolically-labeled transcripts which originated from the start of transcription and extended well beyond promoter-proximal pause site (10). We therefore propose that following CDK12 inhibition, activation of P-TEFb triggers the release of Pol II from pausing at induced genes. As paused Pol II interferes with transcription initiation *in cis* (81), the P-TEFb-driven transition of Pol II into early elongation could enable subsequent bursts of Pol II initiation at induced genes, augmenting further their transcriptional output. It remains to be determined how exactly does the inhibition of CDK12 prompts the release of P-TEFb from 7SK snRNP. We speculate that a phosphoprotein phosphatase PPM1G could be a good candidate for this role. Namely, induction of DSBs triggers ATM-dependent interaction of 7SK with PPM1G (82), of which catalytic activity is crucial to stimulate the release of P-TEFb (83).

Our findings clarify the nature and significance of the induced transcriptome in the wake of CDK12 inhibition. We show that the induced genes are enriched with genes stimulated by prominent cancer-related pathways, including p53, NF-κB, hypoxia and MYC. Supporting these findings, GSEA of hallmark pathways against the DepMap dataset of ranked genetic co-dependencies of *CDK12* across the genome revealed that the effect of *CDK12* knockout on cancer cell growth correlates positively with the oncogenic NF-κB and hypoxia pathways and negatively with the tumor suppressive p53 pathway (83). Furthermore, CDK12 is required for survival and transformation of MYC-overexpressing cells (22,84). By focusing on the p53 and NF-kB pathways, the chief elements of the cellular DDR, we reveal that gene induction in CDK12-targeted cells is functionally important and a prerequisite for the increased sensitivity of cancer cells to P-TEFb inhibitors. In principle, decreased expression of CDK12-dependent genes could also contribute directly to the augmented dependency of CDK12-inhibited cells on P-TEFb. However, our recent work and findings in this study demonstrate that in the case of p53 and NF-κB pathways, gene induction is the culprit. Namely, to disentangle induced from repressed genes in CDK12-inhibited cells, we selectively activated p53- and NF-κB pathways of the induced transcriptome using the non-genotoxic MDM2 inhibitor Nutlin-3a and TNF-α, respectively, which by itself renders the treated cells highly sensitive to P-TEFb

inhibitors (40). Nevertheless, in the context of CDK12-targeted cells, the attenuated gene transcription could enable gene induction indirectly through the rise of DNA damage such as DSBs, which might prompt stimulation of P-TEFb and signal-responsive genes. Finally, a large body of work has established that Pol II promoter-proximal pausing is prevalent on signal-responsive genes, whereby transcriptional activators recruit P-TEFb to facilitate synchronous release of paused Pol II into productive elongation (85). Intriguingly, all TFs that operate at the endpoint of the top enriched pathways in CDK12-targeted cells, namely NF-κB, HIF1A, MYC and p53, have been reported to stimulate Pol II pause release through P-TEFb (86-89). Taken together, our findings are consistent with a model in which inhibition of CDK12 elicits DNA damage-mediated activation of signaling pathways and P-TEFb, which leads to the capturing of this principal Pol II pause release kinase by pathway-specific TFs on chromatin for coordinate gene activation. Accordingly, we envision that this series of events underwrites the heightened reliance of CDK12 targeted cells on P-TEFb.

Our work offers fresh avenues for combinatorial targeting of CDK12 in cancer. Thus far, down-regulation of CDK12-dependent HR genes is being explored as an approach to eliminate cancer cells, most notably in combination with PARP1 inhibitors or DNA-damaging chemotherapeutics (26,27). However, our results call for therapeutic exploitation of gene induction elicited by the inhibition of CDK12, which exposes novel vulnerabilities as well as resistance mechanisms of cancer cells. First, the targeting of CDK12 reactivates p53 and thus primes the cells for undergoing cell death by apoptosis, which we show can be triggered upon co-inhibition of P-TEFb or CDK7. These results resonate with reported studies demonstrating that activation of the p53 transcriptional program sensitizes cancer cells to selective inhibitors of P-TEFb or CDK7 (40,77). Second, our findings indicate that a host of oncogenic signaling pathways could be induced in CDK12-inhibited cells, cautioning against the therapeutic targeting of CDK12 alone. Rather, by interrogating the DNA damage-induced NF-κB pathway, we provide a proof-of-concept for the combination targeting of CDK12 and oncogenic signaling. We demonstrate that the stimulation of the NF-κB pathway alone by TNF-α triggers cell death in combination with P-TEFb inhibitors. Critically, we reveal that the pharmacological targeting of CDK12 in combination with either the transcriptional inhibitors against P-TEFb and CDK7 or inhibitors of IKKβ and ATM of the DNA damage-induced NF-κB pathway, leads to a synergistic drop of cancer cell viability. Importantly, these co-treatments remain effectual in the absence of p53, which is highly relevant from a therapeutic standpoint as up to a half of cancer cases carry loss-of-function mutations in both alleles of *TP53*. As activation of NF-κB has been linked to the resistance of ovarian cancer cells to PARP1 inhibitors (90), targeting this pathway could improve the outcome of the CDK12-PARP1 combination therapy. Finally, we find that the inhibition of ATM prevents the synthetic lethality of CDK12 and P-TEFb co-targeting in p53-proficient cells while it synergizes with CDK12 inhibition in p53-deficient cells. Therefore, we provide further credence to the fact that the functionality of *ATM* and *TP53*, two commonly mutated tumor suppressor genes, is a key determinant of the clinical response to genotoxic chemotherapies. Namely, while cancer cells with functional p53 display chemoresistance upon inhibition of ATM or its downstream target Chk2, inhibition of ATM sensitizes p53-deficient cancer cells to chemotherapy (91). Hence, we propose that the combined status of *ATM* and *TP53* is likely to dictate the efficacy of the CDK12-targeted combination therapies. Conversely, CDK12-deficient tumors could be particularly susceptible to the targeting of P-TEFb, CDK7 and the DNA damage-induced ATM-Chk2 pathway.

Finally, our work uncovers new insights into the tumor suppressive role of CDK12 in the genesis of cancers with biallelic *CDK12* inactivation such as in high-grade serous ovarian carcinoma (28-30). On the one hand, disruption of CDK12-dependent regulatory networks elicits a genomic disarray with the characteristic tandem DNA duplications. On the other hand, our results suggest that *CDK12* loss of heterozygosity engenders the incipient cancer cells with augmented oncogenic signaling that drive key hallmarks of cancer, which in the case of NF-kB signaling include sustained proliferative signaling, avoidance of programmed cell death, tumor-promoting inflammation and therapy resistance (69). Therefore, future exploration of processes driven by perturbation of CDK12 shall reveal the full potential of therapeutic targeting of this crucial Pol II elongation kinase in cancer.

DATA AVAILABILITY

All data associated with this study are presented in the main manuscript or the Supplementary Data. Materials that support the findings of this study are available from the corresponding author upon request.

FUNDING

This work was supported by Sigrid Juselius Foundation [4707979 to M.B.]; Academy of Finland [1309846 to M.B.]; Cancer Society of Finland [4708690 to M.B.]; Deutsche Forschungsgemeinschaft (DFG) in the framework of the Research Unit FOR5200 DEEP-DV (443644894) [FR2938/11-1 to C.C.F.].

CONFLICT OF INTEREST DISCLOSURE

The authors declare no conflict of interest.

ACKNOWLEDGEMENTS

We thank Joaquin M. Espinosa for sharing parental and HCT116 *TP53* $^{-/-}$ cell lines; Dalibor Blazek for sharing HCT116 *CDK12* $^{as/as}$ cell line; Malgorzata Krajewska and Rani E. George for conducting the target engagement assay of Figure 1C; Qiang Zhou for sharing i-CDK9; Nathanael S. Gray for sharing YLK-5-124; HiLife Biomedicum Flow Cytometry Unit at the University of Helsinki for flow cytometry analysis; Monika Mačáková for critical reading of the manuscript.

AUTHOR CONTRIBUTIONS

M.B. conceptualized the study and was assisted by Z.W. in experimental design. M.B. supervised the study. Z.W. performed and analyzed the data of all experiments except the target engagement assay of Figure 1C. C.C.F performed analyses of RNA-seq, TT-seq and 4sU-seq data. M.B. wrote the manuscript with the assistance from Z.W.

REFERENCES

1. Parua, P.K. and Fisher, R.P. (2020) Dissecting the Pol II transcription cycle and derailing cancer with CDK inhibitors. *Nature Chemical Biology*, **16**, 716-724.
2. Eick, D. and Geyer, M. (2013) The RNA polymerase II carboxy-terminal domain (CTD) code. *Chem Rev*, **113**, 8456-8490.
3. Bentley, D.L. (2014) Coupling mRNA processing with transcription in time and space. *Nature Reviews Genetics*, **15**, 163-175.
4. Vos, S.M., Farnung, L., Urlaub, H. and Cramer, P. (2018) Structure of paused transcription complex Pol II-DSIF-NELF. *Nature*, **560**, 601-606.
5. Rimel, J.K., Poss, Z.C., Erickson, B., Maas, Z.L., Ebmeier, C.C., Johnson, J.L., Decker, T.M., Yaron, T.M., Bradley, M.J., Hamman, K.B. *et al.* (2020) Selective inhibition of CDK7 reveals high-confidence targets and new models for TFIIH function in transcription. *Genes Dev*, **34**, 1452-1473.
6. Fujinaga, K., Huang, F. and Peterlin, B.M. (2023) P-TEFb: The master regulator of transcription elongation. *Mol Cell*, **83**, 393-403.
7. Core, L. and Adelman, K. (2019) Promoter-proximal pausing of RNA polymerase II: a nexus of gene regulation. *Genes Dev*, **33**, 960-982.
8. Vos, S.M., Farnung, L., Boehning, M., Wigge, C., Linden, A., Urlaub, H. and Cramer, P. (2018) Structure of activated transcription complex Pol II-DSIF-PAF-SPT6. *Nature*, **560**, 607-612.
9. Blazek, D., Kohoutek, J., Bartholomeeusen, K., Johansen, E., Hulinkova, P., Luo, Z., Cimermancic, P., Ule, J. and Peterlin, B.M. (2011) The Cyclin K/Cdk12 complex maintains genomic stability via regulation of expression of DNA damage response genes. *Genes Dev*, **25**, 2158-2172.
10. Krajewska, M., Dries, R., Grassetti, A.V., Dust, S., Gao, Y., Huang, H., Sharma, B., Day, D.S., Kwiatkowski, N., Pomaville, M. *et al.* (2019) CDK12 loss in cancer cells affects DNA damage response genes through premature cleavage and polyadenylation. *Nat Commun*, **10**, 1757.
11. Tellier, M., Zaborowska, J., Caizzi, L., Mohammad, E., Velychko, T., Schwalb, B., Ferrer-Vicens, I., Blears, D., Nojima, T., Cramer, P. *et al.* (2020) CDK12 globally stimulates RNA polymerase II transcription elongation and carboxyl-terminal domain phosphorylation. *Nucleic Acids Res*, **48**, 7712-7727.
12. Fan, Z., Devlin, J.R., Hogg, S.J., Doyle, M.A., Harrison, P.F., Todorovski, I., Cluse, L.A., Knight, D.A., Sandow, J.J., Gregory, G. *et al.* (2020) CDK13 cooperates with CDK12 to control global RNA polymerase II processivity. *Sci Adv*, **6**.
13. Barboric, M., Lenasi, T., Chen, H., Johansen, E.B., Guo, S. and Peterlin, B.M. (2009) 7SK snRNP/P-TEFb couples transcription elongation with alternative splicing and is essential for vertebrate development. *Proc Natl Acad Sci U S A*, **106**, 7798-7803.
14. Tien, J.F., Mazloomian, A., Cheng, S.G., Hughes, C.S., Chow, C.C.T., Canapi, L.T., Oloumi, A., Trigo-Gonzalez, G., Bashashati, A., Xu, J. *et al.* (2017) CDK12 regulates alternative last exon mRNA splicing and promotes breast cancer cell invasion. *Nucleic Acids Res*, **45**, 6698-6716.
15. Magnuson, B., Bedi, K., Narayanan, I.V., Bartkowiak, B., Blinkiewicz, H., Paulsen, M.T., Greenleaf, A. and Ljungman, M. (2022) CDK12 regulates co-transcriptional splicing and RNA turnover in human cells. *iScience*, **25**, 105030.
16. Parua, P.K., Kalan, S., Benjamin, B., Sanso, M. and Fisher, R.P. (2020) Distinct Cdk9-phosphatase switches act at the beginning and end of elongation by RNA polymerase II. *Nat Commun*, **11**, 4338.
17. Tellier, M., Zaborowska, J., Neve, J., Nojima, T., Hester, S., Fournier, M., Furger, A. and Murphy, S. (2022) CDK9 and PP2A regulate RNA polymerase II transcription termination and coupled RNA maturation. *EMBO Rep*, **23**, e54520.

18. Donovan, M.G., Galbraith, M.D. and Espinosa, J.M. (2022) Multi-omics investigation reveals functional specialization of transcriptional cyclin dependent kinases in cancer biology. *Sci Rep*, **12**, 22505.
19. Pilarova, K., Herudek, J. and Blazek, D. (2020) CDK12: cellular functions and therapeutic potential of versatile player in cancer. *NAR Cancer*, **2**, zcaa003.
20. Dubbury, S.J., Boutz, P.L. and Sharp, P.A. (2018) CDK12 regulates DNA repair genes by suppressing intronic polyadenylation. *Nature*, **564**, 141-145.
21. Chirackal Manavalan, A.P., Pilarova, K., Kluge, M., Bartholomeeusen, K., Rajecky, M., Oppelt, J., Khirsariya, P., Paruch, K., Krejci, L., Friedel, C.C. *et al.* (2019) CDK12 controls G1/S progression by regulating RNAPII processivity at core DNA replication genes. *EMBO Rep*, **20**, e47592.
22. Choi, S.H., Martinez, T.F., Kim, S., Donaldson, C., Shokhirev, M.N., Saghatelian, A. and Jones, K.A. (2019) CDK12 phosphorylates 4E-BP1 to enable mTORC1-dependent translation and mitotic genome stability. *Genes Dev*, **33**, 418-435.
23. Popova, T., Manie, E., Boeva, V., Battistella, A., Goundiam, O., Smith, N.K., Mueller, C.R., Raynal, V., Mariani, O., Sastre-Garau, X. *et al.* (2016) Ovarian Cancers Harboring Inactivating Mutations in CDK12 Display a Distinct Genomic Instability Pattern Characterized by Large Tandem Duplications. *Cancer Res*, **76**, 1882-1891.
24. Menghi, F., Barthel, F.P., Yadav, V., Tang, M., Ji, B., Tang, Z., Carter, G.W., Ruan, Y., Scully, R., Verhaak, R.G.W. *et al.* (2018) The Tandem Duplicator Phenotype Is a Prevalent Genome-Wide Cancer Configuration Driven by Distinct Gene Mutations. *Cancer Cell*, **34**, 197-210 e195.
25. Bajrami, I., Frankum, J.R., Konde, A., Miller, R.E., Rehman, F.L., Brough, R., Campbell, J., Sims, D., Rafiq, R., Hooper, S. *et al.* (2014) Genome-wide profiling of genetic synthetic lethality identifies CDK12 as a novel determinant of PARP1/2 inhibitor sensitivity. *Cancer Res*, **74**, 287-297.
26. Quereda, V., Bayle, S., Vena, F., Frydman, S.M., Monastyrskyi, A., Roush, W.R. and Duckett, D.R. (2019) Therapeutic Targeting of CDK12/CDK13 in Triple-Negative Breast Cancer. *Cancer Cell*, **36**, 545-558 e547.
27. Johnson, S.F., Cruz, C., Greifenberg, A.K., Dust, S., Stover, D.G., Chi, D., Primack, B., Cao, S., Bernhardy, A.J., Coulson, R. *et al.* (2016) CDK12 Inhibition Reverses De Novo and Acquired PARP Inhibitor Resistance in BRCA Wild-Type and Mutated Models of Triple-Negative Breast Cancer. *Cell Rep*, **17**, 2367-2381.
28. Cancer Genome Atlas Research, N. (2011) Integrated genomic analyses of ovarian carcinoma. *Nature*, **474**, 609-615.
29. Ekumi, K.M., Paculova, H., Lenasi, T., Pospichalova, V., Bosken, C.A., Rybarikova, J., Bryja, V., Geyer, M., Blazek, D. and Barboric, M. (2015) Ovarian carcinoma CDK12 mutations misregulate expression of DNA repair genes via deficient formation and function of the Cdk12/CycK complex. *Nucleic Acids Res*, **43**, 2575-2589.
30. Joshi, P.M., Sutor, S.L., Huntoon, C.J. and Karnitz, L.M. (2014) Ovarian cancer-associated mutations disable catalytic activity of CDK12, a kinase that promotes homologous recombination repair and resistance to cisplatin and poly(ADP-ribose) polymerase inhibitors. *J Biol Chem*, **289**, 9247-9253.
31. Choi, H.J., Jin, S., Cho, H., Won, H.Y., An, H.W., Jeong, G.Y., Park, Y.U., Kim, H.Y., Park, M.K., Son, T. *et al.* (2019) CDK12 drives breast tumor initiation and trastuzumab resistance via WNT and IRS1-ErbB-PI3K signaling. *EMBO Rep*, **20**, e48058.
32. Houles, T., Lavoie, G., Nourreddine, S., Cheung, W., Vaillancourt-Jean, E., Guerin, C.M., Bouttier, M., Grondin, B., Lin, S., Saba-El-Leil, M.K. *et al.* (2022) CDK12 is hyperactivated and a synthetic-lethal target in BRAF-mutated melanoma. *Nat Commun*, **13**, 6457.
33. Chou, J., Quigley, D.A., Robinson, T.M., Feng, F.Y. and Ashworth, A. (2020) Transcription-Associated Cyclin-Dependent Kinases as Targets and Biomarkers for Cancer Therapy. *Cancer Discov*, **10**, 351-370.
34. Shan, W., Yuan, J., Hu, Z., Jiang, J., Wang, Y., Loo, N., Fan, L., Tang, Z., Zhang, T., Xu, M. *et al.* (2020) Systematic Characterization of Recurrent Genomic Alterations in Cyclin-

Dependent Kinases Reveals Potential Therapeutic Strategies for Cancer Treatment. *Cell Rep*, **32**, 107884.
35. Vervoort, S.J., Devlin, J.R., Kwiatkowski, N., Teng, M., Gray, N.S. and Johnstone, R.W. (2022) Targeting transcription cycles in cancer. *Nature Reviews Cancer*, **22**, 5-24.
36. Blake, D.R., Vaseva, A.V., Hodge, R.G., Kline, M.P., Gilbert, T.S.K., Tyagi, V., Huang, D., Whiten, G.C., Larson, J.E., Wang, X. *et al.* (2019) Application of a MYC degradation screen identifies sensitivity to CDK9 inhibitors in KRAS-mutant pancreatic cancer. *Sci Signal*, **12**.
37. Loven, J., Hoke, H.A., Lin, C.Y., Lau, A., Orlando, D.A., Vakoc, C.R., Bradner, J.E., Lee, T.I. and Young, R.A. (2013) Selective inhibition of tumor oncogenes by disruption of super-enhancers. *Cell*, **153**, 320-334.
38. Boffo, S., Damato, A., Alfano, L. and Giordano, A. (2018) CDK9 inhibitors in acute myeloid leukemia. *J Exp Clin Cancer Res*, **37**, 36.
39. Ji, X., Lu, H., Zhou, Q. and Luo, K. (2014) LARP7 suppresses P-TEFb activity to inhibit breast cancer progression and metastasis. *Elife*, **3**, e02907.
40. Wang, Z., Macakova, M., Bugai, A., Kuznetsov, S.G., Hassinen, A., Lenasi, T., Potdar, S., Friedel, C.C. and Barboric, M. (2023) P-TEFb promotes cell survival upon p53 activation by suppressing intrinsic apoptosis pathway. *Nucleic Acids Res*, **51**, 1687-1706.
41. Zhang, H., Pandey, S., Travers, M., Sun, H., Morton, G., Madzo, J., Chung, W., Khowsathit, J., Perez-Leal, O., Barrero, C.A. *et al.* (2018) Targeting CDK9 Reactivates Epigenetically Silenced Genes in Cancer. *Cell*, **175**, 1244-1258 e1226.
42. Bacon, C.W. and D'Orso, I. (2018) CDK9: A Signaling Hub for Transcriptional Control. *Transcription*.
43. Quaresma, A.J.C., Bugai, A. and Barboric, M. (2016) Cracking the control of RNA polymerase II elongation by 7SK snRNP and P-TEFb. *Nucleic Acids Res*, **44**, 7527-7539.
44. Olson, S.W., Turner, A.W., Arney, J.W., Saleem, I., Weidmann, C.A., Margolis, D.M., Weeks, K.M. and Mustoe, A.M. (2022) Discovery of a large-scale, cell-state-responsive allosteric switch in the 7SK RNA using DANCE-MaP. *Mol Cell*, **82**, 1708-1723 e1710.
45. Andrade-Lima, L.C., Veloso, A., Paulsen, M.T., Menck, C.F. and Ljungman, M. (2015) DNA repair and recovery of RNA synthesis following exposure to ultraviolet light are delayed in long genes. *Nucleic Acids Res*, **43**, 2744-2756.
46. Williamson, L., Saponaro, M., Boeing, S., East, P., Mitter, R., Kantidakis, T., Kelly, G.P., Lobley, A., Walker, J., Spencer-Dene, B. *et al.* (2017) UV Irradiation Induces a Non-coding RNA that Functionally Opposes the Protein Encoded by the Same Gene. *Cell*, **168**, 843-855 e813.
47. Bugai, A., Quaresma, A.J.C., Friedel, C.C., Lenasi, T., Duster, R., Sibley, C.R., Fujinaga, K., Kukanja, P., Hennig, T., Blasius, M. *et al.* (2019) P-TEFb Activation by RBM7 Shapes a Pro-survival Transcriptional Response to Genotoxic Stress. *Mol Cell*, **74**, 254-267 e210.
48. Studniarek, C., Tellier, M., Martin, P.G.P., Murphy, S., Kiss, T. and Egloff, S. (2021) The 7SK/P-TEFb snRNP controls ultraviolet radiation-induced transcriptional reprogramming. *Cell Rep*, **35**, 108965.
49. Benjamini, Y. and Hochberg, Y. (1995) Controlling the False Discovery Rate: A Practical and Powerful Approach to Multiple Testing. *Journal of the Royal Statistical Society. Series B (Methodological)*, **57**, 289-300.
50. Subramanian, A., Tamayo, P., Mootha Vamsi, K., Mukherjee, S., Ebert Benjamin, L., Gillette Michael, A., Paulovich, A., Pomeroy Scott, L., Golub Todd, R., Lander Eric, S. *et al.* (2005) Gene set enrichment analysis: A knowledge-based approach for interpreting genome-wide expression profiles. *Proceedings of the National Academy of Sciences*, **102**, 15545-15550.
51. Zhang, T., Kwiatkowski, N., Olson, C.M., Dixon-Clarke, S.E., Abraham, B.J., Greifenberg, A.K., Ficarro, S.B., Elkins, J.M., Liang, Y., Hannett, N.M. *et al.* (2016) Covalent targeting of remote cysteine residues to develop CDK12 and CDK13 inhibitors. *Nat Chem Biol*, **12**, 876-884.
52. Kwiatkowski, N., Zhang, T., Rahl, P.B., Abraham, B.J., Reddy, J., Ficarro, S.B., Dastur, A., Amzallag, A., Ramaswamy, S., Tesar, B. *et al.* (2014) Targeting transcription regulation in cancer with a covalent CDK7 inhibitor. *Nature*, **511**, 616-620.

53. Liang, K., Gao, X., Gilmore, J.M., Florens, L., Washburn, M.P., Smith, E. and Shilatifard, A. (2015) Characterization of human cyclin-dependent kinase 12 (CDK12) and CDK13 complexes in C-terminal domain phosphorylation, gene transcription, and RNA processing. *Mol Cell Biol*, **35**, 928-938.
54. McKay, B.C., Stubbert, L.J., Fowler, C.C., Smith, J.M., Cardamore, R.A. and Spronck, J.C. (2004) Regulation of ultraviolet light-induced gene expression by gene size. *Proc Natl Acad Sci U S A*, **101**, 6582-6586.
55. Li, X., Huang, C.-H., Sánchez-Rivera, F.J., Kennedy, M.C., Tschaharganeh, D.F., Morris, J.P., Montinaro, A., O'Rourke, K.P., Banito, A., Wilkinson, J.E. *et al.* (2022) A preclinical platform for assessing antitumor effects and systemic toxicities of cancer drug targets. **119**, e2110557119.
56. Olson, C.M., Jiang, B., Erb, M.A., Liang, Y., Doctor, Z.M., Zhang, Z., Zhang, T., Kwiatkowski, N., Boukhali, M., Green, J.L. *et al.* (2018) Pharmacological perturbation of CDK9 using selective CDK9 inhibition or degradation. *Nat Chem Biol*, **14**, 163-170.
57. Liberzon, A., Birger, C., Thorvaldsdóttir, H., Ghandi, M., Mesirov, J.P. and Tamayo, P. (2015) The Molecular Signatures Database (MSigDB) hallmark gene set collection. *Cell Syst*, **1**, 417-425.
58. Shiloh, Y. and Ziv, Y. (2013) The ATM protein kinase: regulating the cellular response to genotoxic stress, and more. *Nat Rev Mol Cell Biol*, **14**, 197-210.
59. Bencokova, Z., Kaufmann, M.R., Pires, I.M., Lecane, P.S., Giaccia, A.J. and Hammond, E.M. (2009) ATM activation and signaling under hypoxic conditions. *Mol Cell Biol*, **29**, 526-537.
60. Campaner, S. and Amati, B. (2012) Two sides of the Myc-induced DNA damage response: from tumor suppression to tumor maintenance. *Cell Div*, **7**, 6.
61. Hadian, K. and Krappmann, D. (2011) Signals from the nucleus: activation of NF-kappaB by cytosolic ATM in the DNA damage response. *Sci Signal*, **4**, pe2.
62. Lavin, M.F. and Gueven, N. (2006) The complexity of p53 stabilization and activation. *Cell Death Differ*, **13**, 941-950.
63. Fang, L., Choudhary, S., Zhao, Y., Edeh, C.B., Yang, C., Boldogh, I. and Brasier, A.R. (2014) ATM regulates NF-kappaB-dependent immediate-early genes via RelA Ser 276 phosphorylation coupled to CDK9 promoter recruitment. *Nucleic Acids Res*, **42**, 8416-8432.
64. Golding, S.E., Rosenberg, E., Valerie, N., Hussaini, I., Frigerio, M., Cockcroft, X.F., Chong, W.Y., Hummersone, M., Rigoreau, L., Menear, K.A. *et al.* (2009) Improved ATM kinase inhibitor KU-60019 radiosensitizes glioma cells, compromises insulin, AKT and ERK prosurvival signaling, and inhibits migration and invasion. *Mol Cancer Ther*, **8**, 2894-2902.
65. Sur, S., Pagliarini, R., Bunz, F., Rago, C., Diaz, L.A., Jr., Kinzler, K.W., Vogelstein, B. and Papadopoulos, N. (2009) A panel of isogenic human cancer cells suggests a therapeutic approach for cancers with inactivated p53. *Proceedings of the National Academy of Sciences of the United States of America*, **106**, 3964-3969.
66. Kastenhuber, E.R. and Lowe, S.W. (2017) Putting p53 in Context. *Cell*, **170**, 1062-1078.
67. Dixon, A.S., Schwinn, M.K., Hall, M.P., Zimmerman, K., Otto, P., Lubben, T.H., Butler, B.L., Binkowski, B.F., Machleidt, T., Kirkland, T.A. *et al.* (2016) NanoLuc Complementation Reporter Optimized for Accurate Measurement of Protein Interactions in Cells. *ACS Chem Biol*, **11**, 400-408.
68. Zanoni, M., Piccinini, F., Arienti, C., Zamagni, A., Santi, S., Polico, R., Bevilacqua, A. and Tesei, A. (2016) 3D tumor spheroid models for in vitro therapeutic screening: a systematic approach to enhance the biological relevance of data obtained. *Sci Rep*, **6**, 19103.
69. Taniguchi, K. and Karin, M. (2018) NF-kappaB, inflammation, immunity and cancer: coming of age. *Nat Rev Immunol*, **18**, 309-324.
70. Zatzman, M., Fuligni, F., Ripsman, R., Suwal, T., Comitani, F., Edward, L.-M., Denroche, R., Jang, G.H., Notta, F., Gallinger, S. *et al.* (2022) Widespread hypertranscription in aggressive human cancers. *Science Advances*, **8**, eabn0238.
71. Hideshima, T., Neri, P., Tassone, P., Yasui, H., Ishitsuka, K., Raje, N., Chauhan, D., Podar, K., Mitsiades, C., Dang, L. *et al.* (2006) MLN120B, a novel IkappaB kinase beta inhibitor, blocks multiple myeloma cell growth in vitro and in vivo. *Clin Cancer Res*, **12**, 5887-5894.

72. Fisher, R.P. (2012) The CDK Network: Linking Cycles of Cell Division and Gene Expression. *Genes Cancer*, **3**, 731-738.
73. Schachter, M.M., Merrick, K.A., Larochelle, S., Hirschi, A., Zhang, C., Shokat, K.M., Rubin, S.M. and Fisher, R.P. (2013) A Cdk7-Cdk4 T-loop phosphorylation cascade promotes G1 progression. *Mol Cell*, **50**, 250-260.
74. Olson, C.M., Liang, Y., Leggett, A., Park, W.D., Li, L., Mills, C.E., Elsarrag, S.Z., Ficarro, S.B., Zhang, T., Duster, R. *et al.* (2019) Development of a Selective CDK7 Covalent Inhibitor Reveals Predominant Cell-Cycle Phenotype. *Cell Chem Biol*, **26**, 792-803 e710.
75. Carneiro, B.A. and El-Deiry, W.S. (2020) Targeting apoptosis in cancer therapy. *Nature Reviews Clinical Oncology*, **17**, 395-417.
76. Bai, L. and Wang, S. (2014) Targeting Apoptosis Pathways for New Cancer Therapeutics. *Annual Review of Medicine*, **65**, 139-155.
77. Kalan, S., Amat, R., Schachter, M.M., Kwiatkowski, N., Abraham, B.J., Liang, Y., Zhang, T., Olson, C.M., Larochelle, S., Young, R.A. *et al.* (2017) Activation of the p53 Transcriptional Program Sensitizes Cancer Cells to Cdk7 Inhibitors. *Cell Rep*, **21**, 467-481.
78. Chipumuro, E., Marco, E., Christensen, C.L., Kwiatkowski, N., Zhang, T., Hatheway, C.M., Abraham, B.J., Sharma, B., Yeung, C., Altabef, A. *et al.* (2014) CDK7 inhibition suppresses super-enhancer-linked oncogenic transcription in MYCN-driven cancer. *Cell*, **159**, 1126-1139.
79. Zeng, M., Kwiatkowski, N.P., Zhang, T., Nabet, B., Xu, M., Liang, Y., Quan, C., Wang, J., Hao, M., Palakurthi, S. *et al.* (2018) Targeting MYC dependency in ovarian cancer through inhibition of CDK7 and CDK12/13. *Elife*, **7**.
80. Jaeger, M.G., Schwalb, B., Mackowiak, S.D., Velychko, T., Hanzl, A., Imrichova, H., Brand, M., Agerer, B., Chorn, S., Nabet, B. *et al.* (2020) Selective Mediator dependence of cell-type-specifying transcription. *Nat Genet*, **52**, 719-727.
81. Gressel, S., Schwalb, B., Decker, T.M., Qin, W., Leonhardt, H., Eick, D. and Cramer, P. (2017) CDK9-dependent RNA polymerase II pausing controls transcription initiation. *Elife*, **6**.
82. Gudipaty, S.A., McNamara, R.P., Morton, E.L. and D'Orso, I. (2015) PPM1G Binds 7SK RNA and Hexim1 To Block P-TEFb Assembly into the 7SK snRNP and Sustain Transcription Elongation. *Mol Cell Biol*, **35**, 3810-3828.
83. McNamara, R.P., McCann, J.L., Gudipaty, S.A. and D'Orso, I. (2013) Transcription factors mediate the enzymatic disassembly of promoter-bound 7SK snRNP to locally recruit P-TEFb for transcription elongation. *Cell Rep*, **5**, 1256-1268.
84. Toyoshima, M., Howie, H.L., Imakura, M., Walsh, R.M., Annis, J.E., Chang, A.N., Frazier, J., Chau, B.N., Loboda, A., Linsley, P.S. *et al.* (2012) Functional genomics identifies therapeutic targets for MYC-driven cancer. *Proc Natl Acad Sci U S A*, **109**, 9545-9550.
85. Liu, X., Kraus, W.L. and Bai, X. (2015) Ready, pause, go: regulation of RNA polymerase II pausing and release by cellular signaling pathways. *Trends Biochem Sci*, **40**, 516-525.
86. Barboric, M., Nissen, R.M., Kanazawa, S., Jabrane-Ferrat, N. and Peterlin, B.M. (2001) NF-kappaB binds P-TEFb to stimulate transcriptional elongation by RNA polymerase II. *Mol Cell*, **8**, 327-337.
87. Galbraith, M.D., Allen, M.A., Bensard, C.L., Wang, X., Schwinn, M.K., Qin, B., Long, H.W., Daniels, D.L., Hahn, W.C., Dowell, R.D. *et al.* (2013) HIF1A employs CDK8-mediator to stimulate RNAPII elongation in response to hypoxia. *Cell*, **153**, 1327-1339.
88. Kanazawa, S., Soucek, L., Evan, G., Okamoto, T. and Peterlin, B.M. (2003) c-Myc recruits P-TEFb for transcription, cellular proliferation and apoptosis. *Oncogene*, **22**, 5707-5711.
89. Albert, T.K., Antrecht, C., Kremmer, E. and Meisterernst, M. (2016) The Establishment of a Hyperactive Structure Allows the Tumour Suppressor Protein p53 to Function through P-TEFb during Limited CDK9 Kinase Inhibition. *PLoS One*, **11**, e0146648.
90. Ma, H., Qi, G., Han, F., Peng, J., Yuan, C. and Kong, B. (2022) PBK drives PARP inhibitor resistance through the TRIM37/NFkappaB axis in ovarian cancer. *Exp Mol Med*, **54**, 999-1010.
91. Jiang, H., Reinhardt, H.C., Bartkova, J., Tommiska, J., Blomqvist, C., Nevanlinna, H., Bartek, J., Yaffe, M.B. and Hemann, M.T. (2009) The combined status of ATM and p53 link tumor development with therapeutic response. *Genes Dev*, **23**, 1895-1909.

FIGURES AND FIGURE LEGENDS

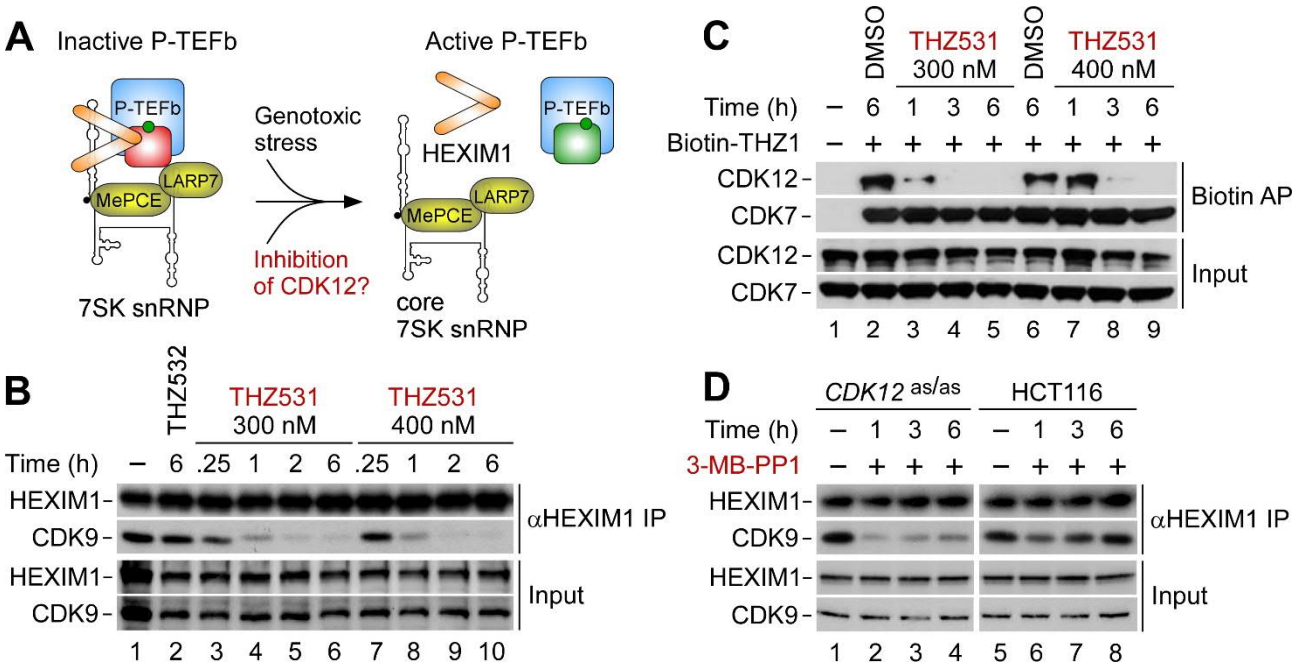

Figure 1. Inhibition of CDK12 triggers the release of P-TEFb from the inhibitory 7SK snRNP complex.

(A) Schematic representation of controlling the kinase activity of P-TEFb with 7SK snRNP. Upon the release of inactive P-TEFb (CDK9 in red) from 7SK snRNP, the interaction of P-TEFb with HEXIM1 does not take place, resulting in the activation of P-TEFb (CDK9 in green). For simplicity, a large-scale conformational switching of 7SK upon the release of P-TEFb from the core of 7SK snRNP is not depicted.

(B) CoIP of HEXIM1 with CDK9 from whole cell extracts of HCT116 cells. Cells were treated with DMSO (-), THZ532 (400 nM) and two different doses of THZ531 for the indicated duration prior to preparation of whole cell extracts and detection of HEXIM1 and CDK9 in HEXIM1 immunoprecipitations (αHEXIM1 IP) and whole cell extracts (Input) by Western blotting.

(C) Specificity of the targeting of CDK12 with THZ531 in target engagement assay. HCT116 cells were treated with DMSO (-) and two different doses of THZ531 for the indicated duration (in hours) prior to preparation of whole cell extracts and detection of CDK12 and CDK7 in Biotin-THZ1 (1μM) affinity purifications (Biotin AP) and whole cell extracts (Input) by Western blotting.

(D) CoIP of HEXIM1 with CDK9 from whole cell extracts of the indicated HCT116 cell lines. Cells were treated with DMSO (-) and 3-MB-PP1 for the indicated duration (in hours) prior to preparation of whole cell extracts and detection of HEXIM1 and CDK9 in HEXIM1 immunoprecipitations (αHEXIM1 IP) and whole cell extracts (Input) by Western blotting.

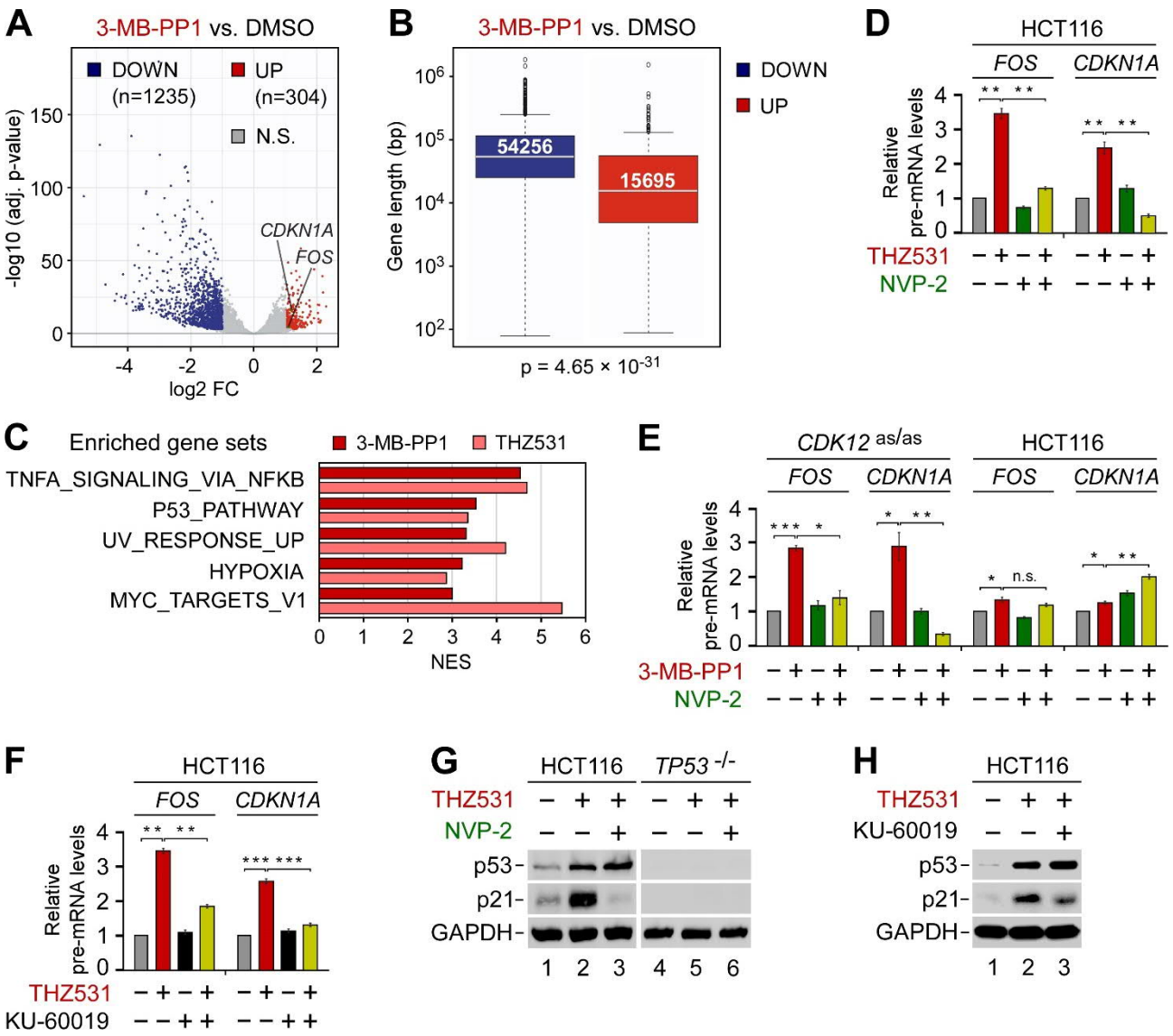

Figure 2. P-TEFb and ATM promote gene induction in CDK12-targeted cells.

(A) Volcano plot representation of differentially expressed genes (n = 12,495; p-adj ≤ 0.001; Log2 FC ≥ 1) from nuclear RNA-seq experiments (n = 3) of HCT116 *CDK12* $^{as/as}$ cells that were synchronized by serum deprivation for 72 h prior to their culture in the serum-containing medium for 4.5 h in the presence of DMSO or 3-MB-PP1 (5 μM). Repressed (DOWN), induced (UP) and non-significantly regulated (N.S.) genes are indicated. NVP-2 sensitive *CDKN1A* and *FOS* are highlighted. FC, fold-change.

(B) Boxplot indicating distribution of gene lengths for the repressed and induced protein-coding genes from (A). Median gene length for each group and p-value are indicated. bp, base pair.

(C) Gene set enrichment analysis of differentially expressed protein-coding genes obtained from RNA-seq experiments (n = 3) of serum-synchronized HCT116 *CDK12* $^{as/as}$ cells treated with DMSO and 3-MB-PP1 (5 μM) for 4.5 h and TT-seq experiments (n = 3) of IMR-32 cells treated with DMSO and THZ531 (400 nM) for 2 h. Top gene sets from the hallmark gene set collection that are associated with induced genes are shown (FDR q-val ≤0.001). NES, normalized enrichment score.

(D-F) HCT116 cell lines were treated with DMSO (-), THZ531 (400 nM), 3-MB-PP1 (5 μM), NVP-2 (20 nM) and KU-60019 (5 μM) alone and in combination as indicated for 3 h prior to quantifying pre-mRNA levels of *FOS* and *CDKN1A* with RT-qPCR. Results normalized to the levels of GAPDH mRNA and DMSO-treated cells are presented as the mean ± s.e.m. (n = 3). *, $P < 0.05$; **, $P < 0.01$; ***, $P < 0.001$, n.s., non-significant, determined by Student's *t* test.

(G,H) HCT116 cell lines were treated with DMSO (-), THZ531 (400 nM), NVP-2 (20 nM) and KU-60019 (5 μM) alone and in combination as indicated for 16 h prior to preparation of whole cell extracts and detection of the indicated proteins by Western blotting.

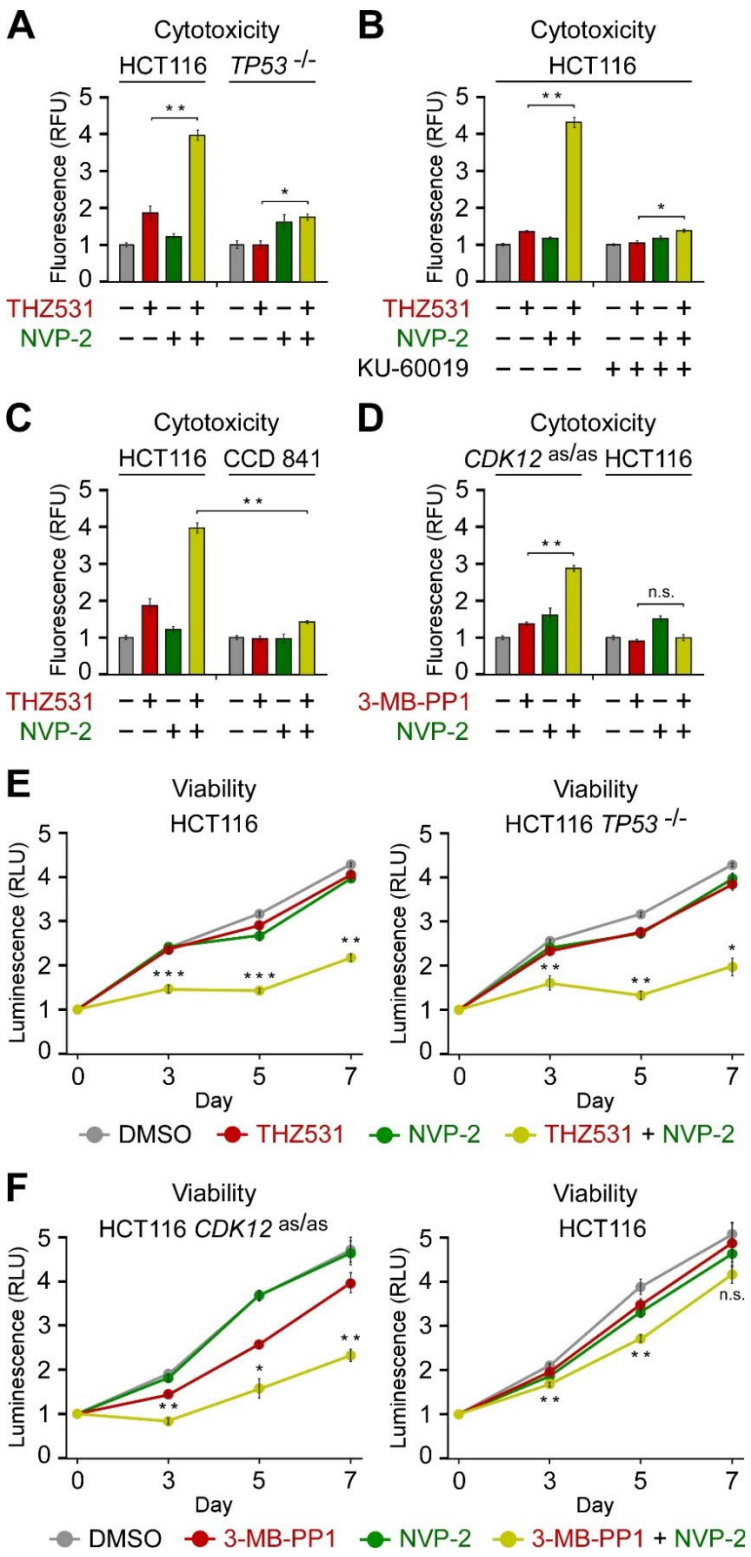

Figure 3. Co-targeting of CDK12 and P-TEFb decreases viability of HCT116 cells.

(A-D) Cytotoxicity of the indicated cell lines treated with DMSO (-), THZ531 (200 nM), 3-MB-PP1 (5 μM), NVP-2 (10 nM) and KU-60019 (5 μM) alone and in combination as indicated for 48 h measured using CellTox Green Cytotoxicity Assay. Results are presented as fluorescence values relative to the values of DMSO-treated cells and plotted as the mean ± s.e.m. (n = 3). *, $P < 0.05$; **, $P < 0.01$; n.s., non-significant, determined by Student's *t* test.

(E) Viability of HCT116 cell lines treated with DMSO, THZ531 (50 nM) and NVP-2 (2.5 nM) alone and in combination as indicated. Results obtained at the time points indicated below the graphs using CellTiter-Glo 2.0 Cell Viability Assay are presented as luminescence values relative to the values at Day 0 and plotted as the mean ± s.e.m. (n = 3). *, $P < 0.05$; **, $P < 0.01$; ***, $P < 0.001$, determined by Student's *t* test using THZ531 and THZ531 + NVP-2 data sets.

(F) Viability of HCT116 cell lines treated with DMSO, 3-MB-PP1 (2.5 μM) and NVP-2 (1.25 nM) alone and in combination as indicated. Results obtained at the time points indicated below the graphs using CellTiter-Glo 2.0 Cell Viability Assay are presented as luminescence values relative to the values at Day 0 and plotted as the mean ± s.e.m. (n = 3). *, $P < 0.05$; **, $P < 0.01$; n.s., non-significant, determined by Student's *t* test using 3-MB-PP1 and 3-MB-PP1 + NVP-2 data sets.

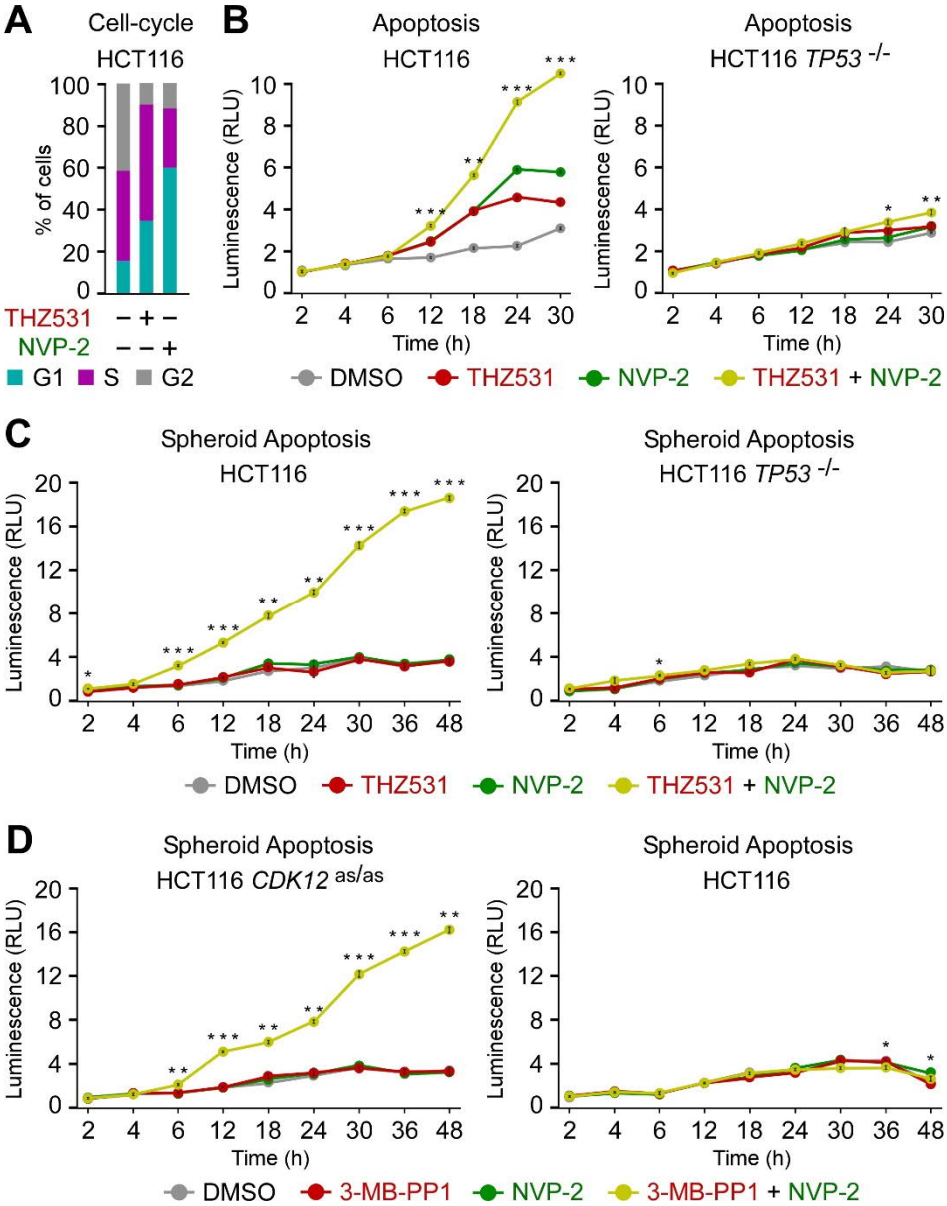

Figure 4. Co-targeting of CDK12 and P-TEFb stimulates p53-dependent apoptosis of HCT116 cells.

(A) Quantification of cells (%) in the indicated cell-cycle phases based on flow cytometry profiles of propidium iodide-stained HCT116 cells that were synchronized by serum deprivation for 24 h prior to their culture in the serum-containing medium for 24 h in the presence of DMSO (-), THZ531 (50 nM) and NVP-2 (50 nM) as indicated.

(B) Apoptosis of HCT116 cell lines treated with DMSO, THZ531 (100 nM) and NVP-2 (10 nM) alone and in combination as indicated. Results obtained at the time points indicated below the graphs using RealTime-Glo Annexin V Apoptosis and Necrosis Assay are presented as luminescence values relative to the values of DMSO-treated cells at 2 h and plotted as the mean ± s.e.m. (n = 3). *, $P < 0.05$; **, $P < 0.01$; ***, $P < 0.001$, determined by Student's *t* test using THZ531 and THZ531 + NVP-2 data sets.

(C,D) Apoptosis of HCT116 cell line spheroid cultures treated with DMSO, THZ531 (100 nM), 3-MB-PP1 (5 μM) and NVP-2 (10 nM) alone and in combination as indicated. Spheroids were formed for

48 h prior to the treatments. Results obtained at the time points indicated below the graphs using RealTime-Glo Annexin V Apoptosis and Necrosis Assay are presented as luminescence values relative to the values of DMSO-treated cells at 2 h and plotted as the mean ± s.e.m. (n = 3). *, $P < 0.05$; **, $P < 0.01$; ***, $P < 0.001$, determined by Student's *t* test using THZ531 and THZ531 + NVP-2 (B), and 3-MB-PP1 and 3-MB-PP1 + NVP-2 (C) data sets.

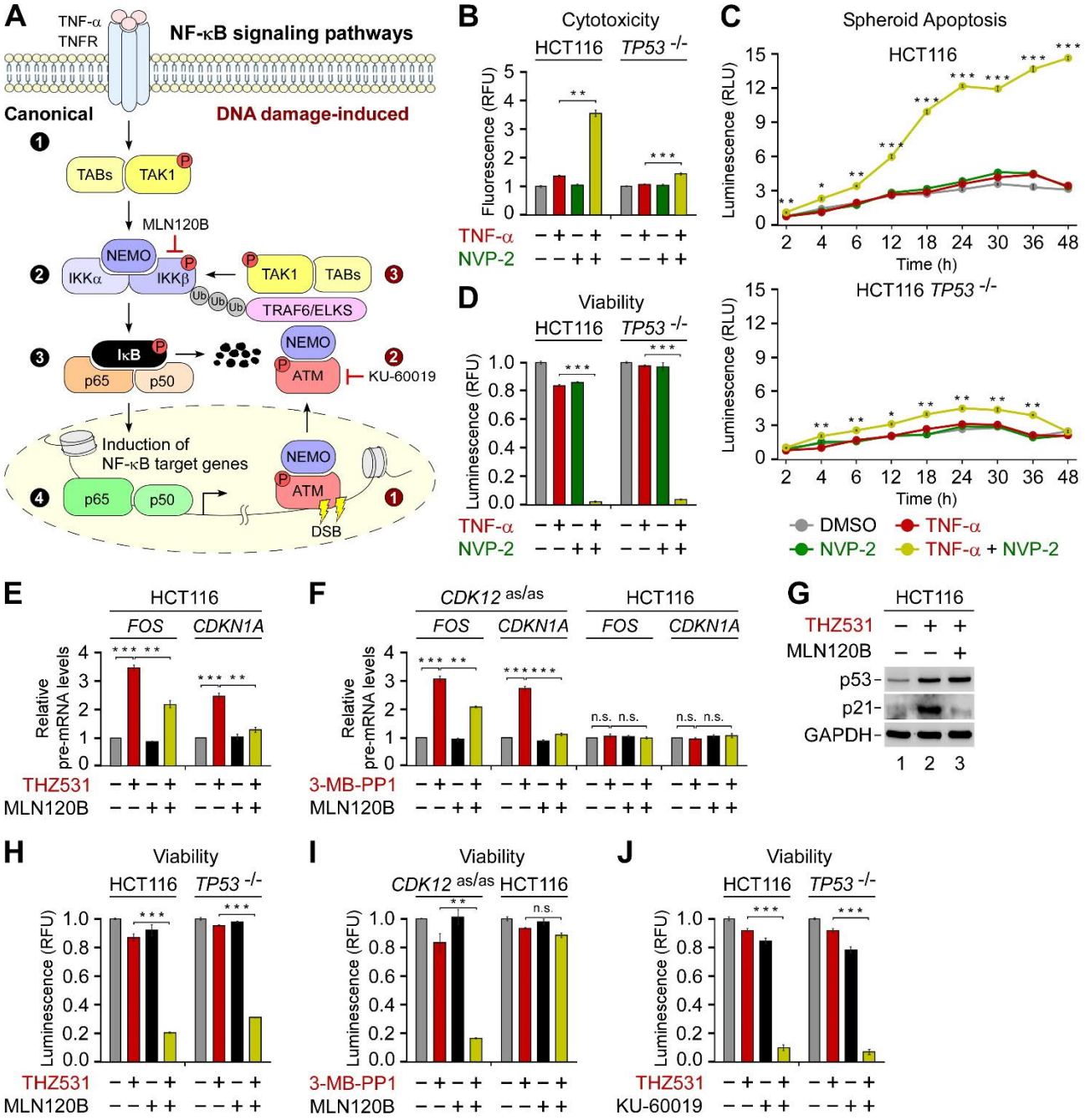

Figure 5. Inhibition of CDK12 renders cancer cells dependent on the NF-κB signaling pathway.

(A) Cartoon depicting key events of the canonical and DNA damage-induced NF-κB signaling pathway. In the canonical pathway, trimerization of TNFRSF1A by TNF-α leads to phosphorylation-induced activation of TAK1 (step 1), which in a complex with TABs phosphorylates and activates IKKβ of the IKK complex (step 2) that also includes a related catalytic subunit IKKβ and a regulatory subunit, NEMO/IKKγ. In turn, IKKβ induces the phosphorylation and degradation of IκBα (step 3), allowing NF-κB to translocate to the nucleus and stimulate proliferative and anti-apoptotic gene transcription program (step 4). In the DNA damage-induced pathway, induction of DSBs activates ATM and stimulates nuclear import of a fraction of NEMO (step 1), after which ATM in a complex with NEMO is exported from the nucleus (step 2) to stimulate TAK1-mediated phosphorylation of

IKKβ within signalosomes formed upon ATM-stimulated auto-polyubiquitylation of TRAF6 and polyubiquitylation of the IKK adaptor ELKS (step 3). Pharmacological targeting of IKKβ by MLN120B and ATM by KU-60019 is indicated. TNF-α, tumor necrosis factor α; TNFRSF1A, TNF receptor superfamily member 1A; TAK1, TGF-β-activated kinase 1; TABs, TAK1 binding proteins; NF-κB, nuclear factor kappa-light-chain-enhancer of activated B cells; IKKα, inhibitor of κB (IκB) kinase α; IKKβ, inhibitor of IκB kinase β; NEMO/IKKγ, NF-κB essential modulator; p65/p50, heterodimer of NF-κB; ATM, ataxia-telangiectasia mutated; TRAF6, tumor necrosis factor receptor–associated factor 6.

(B) Cytotoxicity of HCT116 cell lines treated with DMSO, TNF-α (20 ng/ml) and NVP-2 (10 nM) alone and in combination as indicated for 48 h measured using CellTox Green Cytotoxicity Assay. Results are presented as fluorescence values relative to the values of DMSO-treated cells and plotted as the mean ± s.e.m. (n = 3). **, P < 0.01; ***, P < 0.001, determined by Student's *t* test.

(C) Apoptosis of HCT116 cell line spheroid cultures treated with DMSO, TNF-α (20 ng/ml) and NVP-2 (10 nM) alone and in combination as indicated. Spheroids were formed for 48 h prior to the treatments. Results obtained at the time points indicated below the graphs using RealTime-Glo Annexin V Apoptosis and Necrosis Assay are presented as luminescence values relative to the values of DMSO-treated cells at 2 h and plotted as the mean ± s.e.m. (n = 3). *, P < 0.05; **, P < 0.01; ***, P < 0.001, determined by Student's *t* test using TNF-α and TNF-α + NVP-2 data sets.

(D) Viability of HCT116 cell lines treated with DMSO, TNF-α (5 ng/ml) and NVP-2 (2.5 nM) alone and in combination as indicated for seven days measured using CellTiter-Glo 2.0 Cell Viability Assay. Results are presented as luminescence values relative to the values of DMSO-treated cells and plotted as the mean ± s.e.m. (n = 3). ***, P < 0.001, determined by Student's *t* test.

(E,F) HCT116 cell lines were treated with DMSO (-), THZ531 (400 nM), 3-MB-PP1 (5 μM) and MLN120B (20 μM) alone and in combination as indicated for 3 h prior to quantifying pre-mRNA levels of *FOS* and *CDKN1A* with RT-qPCR. Results normalized to the levels of GAPDH mRNA and DMSO-treated cells are presented as the mean ± s.e.m. (n = 3). *, P < 0.05; **, P < 0.01; ***, P < 0.001, n.s., non-significant, determined by Student's *t* test.

(G) HCT116 cells were treated with DMSO (-), THZ531 (400 nM), NVP-2 (20 nM) and MLN120B (20 μM) alone and in combination as indicated for 16 h prior to preparation of whole cell extracts and detection of the indicated proteins by Western blotting.

(H-J) Viability of HCT116 cell lines treated with DMSO, THZ531 (50 nM), 3-MB-PP1 (2.5 μM), MLN120B (2.5 μM in E; 5 μM in F) and KU-60019 (50 nM) alone and in combination as indicated for seven days measured using CellTiter-Glo 2.0 Cell Viability Assay. Results are presented as luminescence values relative to the values of DMSO-treated cells and plotted as the mean ± s.e.m. (n = 3). **, P < 0.01; ***, P < 0.001; n.s., non-significant, determined by Student's *t* test.

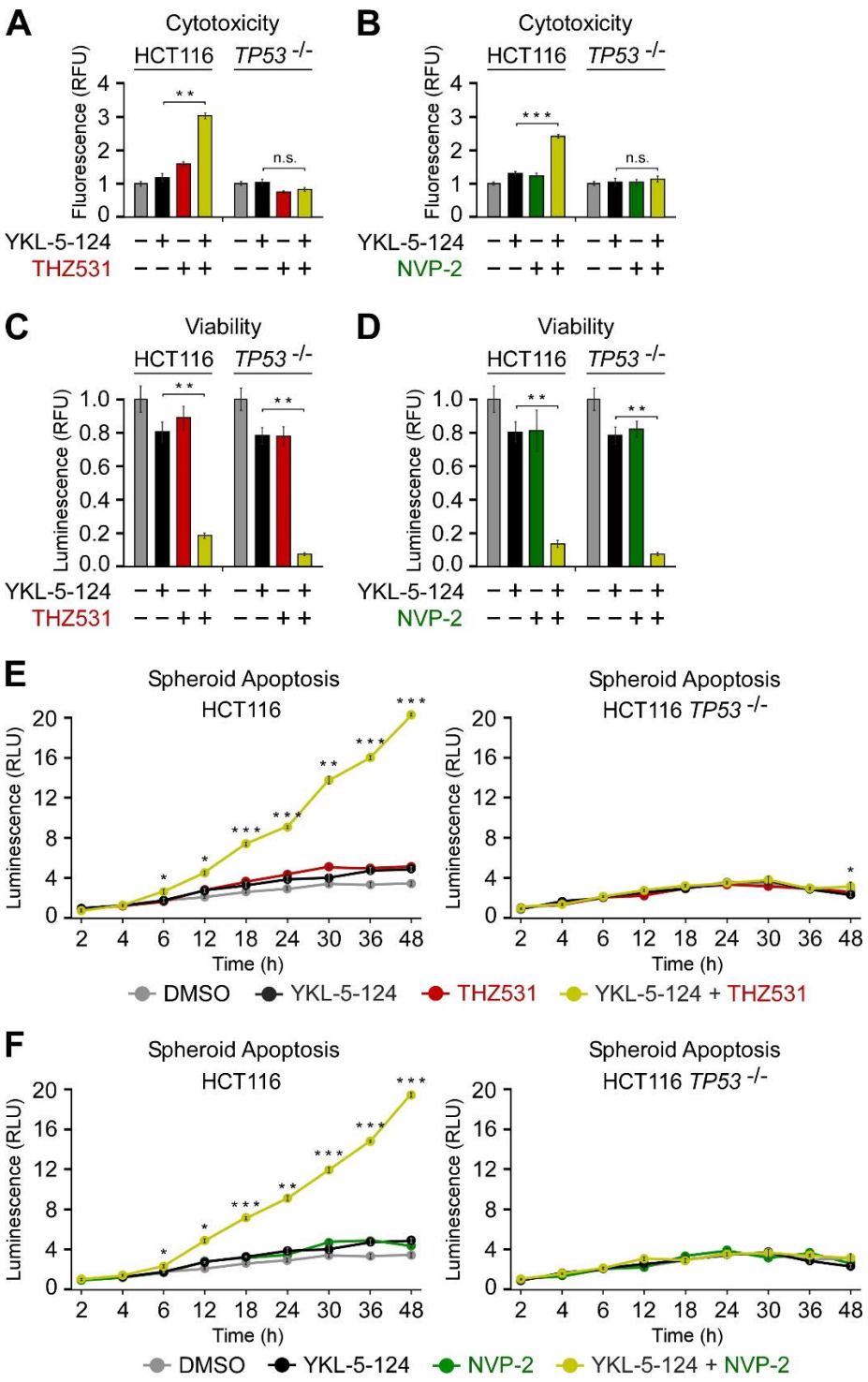

Figure 6. Inhibition of CDK12 or P-TEFb switches the fate of CDK7-inhibited cancer cells from cell-cycle arrest to apoptosis.

(A,B) Cytotoxicity of the indicated HCT116 cell lines treated with DMSO, YKL-5-124 (100 nM), THZ531 (200 nM) and NVP-2 (10 nM) alone and in combination as indicated for 48 h measured using CellTox Green Cytotoxicity Assay. Results are presented as fluorescence values relative to the values of DMSO-treated cells and plotted as the mean ± s.e.m. (n = 3). *, P < 0.05; **, P < 0.01; ***, P < 0.001; n.s., non-significant, determined by Student's *t* test.

(C,D) Viability of the indicated HCT116 cell lines treated with DMSO, YKL-5-124 (5 nM), THZ531 (50 nM) and NVP-2 (2.5 nM) alone and in combination as indicated for seven days measured using CellTiter-Glo 2.0 Cell Viability Assay. Results are presented as luminescence values relative to the values of DMSO-treated cells and plotted as the mean ± s.e.m. (n = 3). **, $P < 0.01$, determined by Student's *t* test.

(E,F) Apoptosis of the indicated HCT116 cell line spheroid cultures treated with DMSO, YKL-5-124 (100 nM), THZ531 (150 nM) and NVP-2 (10 nM) alone and in combination as indicated. Spheroids were formed for 48 h prior to the treatments. Results obtained at the time points indicated below the graphs using RealTime-Glo Annexin V Apoptosis and Necrosis Assay are presented as luminescence values relative to the values of DMSO-treated cells at 2 h and plotted as the mean ± s.e.m. (n = 3). *, $P < 0.05$; **, $P < 0.01$; ***, $P < 0.001$, determined by Student's *t* test using YKL-5-124 and YKL-5-124 + THZ531 (C), and YKL-5-124 and YKL-5-124 + NVP-2 (D) data sets.

SUPPLEMENTARY FIGURES, FIGURE LEGENDS AND TABLES

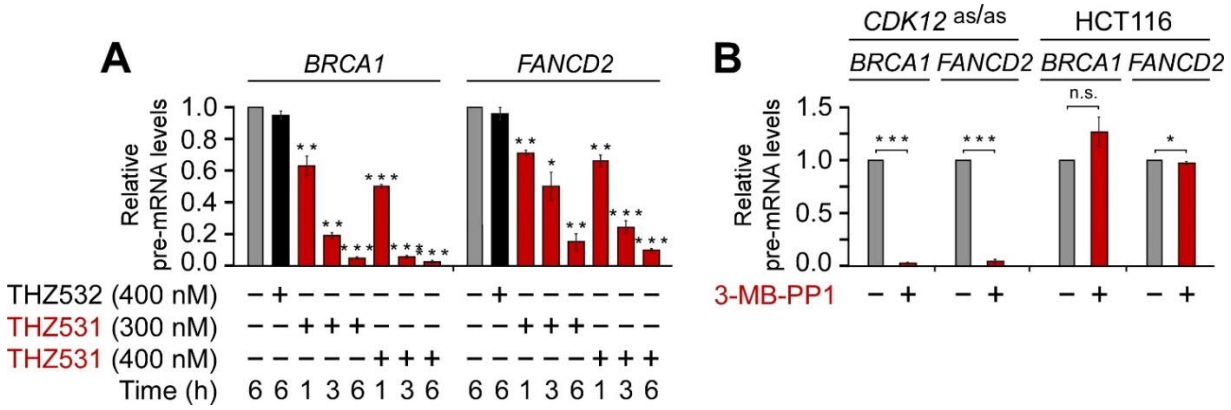

Supplementary Figure S1. Inhibition of CDK12 triggers the release of P-TEFb from the inhibitory 7SK snRNP complex.

(A) HCT116 cells were treated with DMSO (-), THZ532 and two different doses of THZ531 as indicated for the indicated duration prior to quantifying pre-mRNA levels of *BRCA1* and *FANCD2* with RT-qPCR. Results normalized to the levels of GAPDH mRNA and DMSO-treated cells are presented as the mean ± s.e.m. (n = 3). *, P < 0.05; **, P < 0.01; ***, P < 0.001, determined by Student's *t* test.

(B) HCT116 cell lines were treated with DMSO (-) and 3-MB-PP1 (5 μM) as indicated for 3 h prior to quantifying pre-mRNA levels of *BRCA1* and *FANCD2* with RT-qPCR. Results normalized to the levels of GAPDH mRNA and DMSO-treated cells are presented as the mean ± s.e.m. (n = 3). *, P < 0.05; ***, P < 0.001; n.s., non-significant, determined by Student's *t* test.

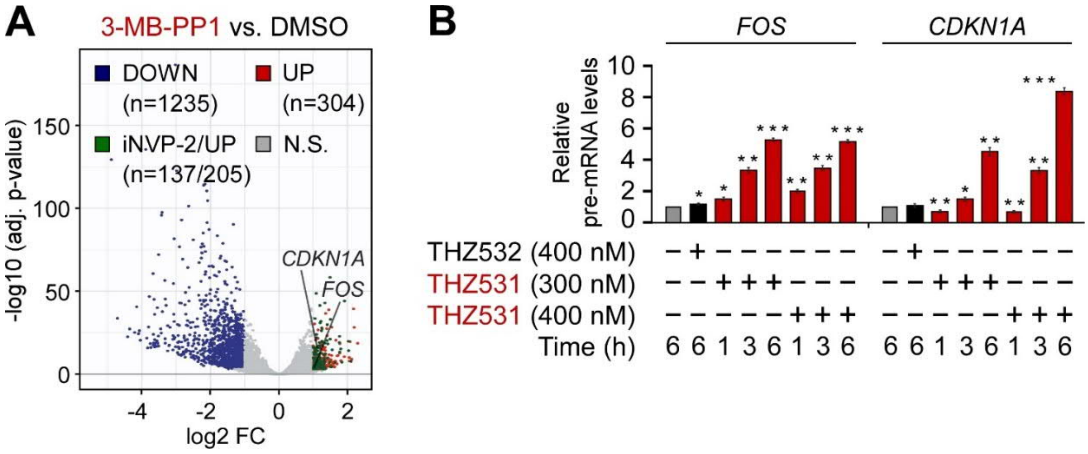

Supplementary Figure S2. P-TEFb and ATM promote gene induction in CDK12-targeted cells.

(A) Volcano plot representation of differentially expressed genes (n = 12,495; p-adj ≤ 0.001; Log2 FC ≥ 1) from nuclear RNA-seq experiments (n = 3) of HCT116 *CDK12* $^{as/as}$ cells that were synchronized by serum deprivation for 72 h prior to their culture in the serum-containing medium for 4.5 h in the presence of DMSO or 3-MB-PP1 (5 μM). Repressed (DOWN), induced (UP), induced and inhibited by NVP-2 (iNVP-2/UP) and non-significantly regulated (N.S.) genes are indicated. NVP-2 sensitive *CDKN1A* and *FOS* are highlighted. FC, fold-change.

(B) HCT116 cells were treated with DMSO, THZ532 and two different doses of THZ531 as indicated for the indicated duration prior to quantifying pre-mRNA levels of *BRCA1* and *FANCD2* with RT-qPCR. Results normalized to the levels of GAPDH mRNA and DMSO-treated cells are presented as the mean ± s.e.m. (n = 3). *, P < 0.05; **, P < 0.01; ***, P < 0.001, determined by Student's *t* test.

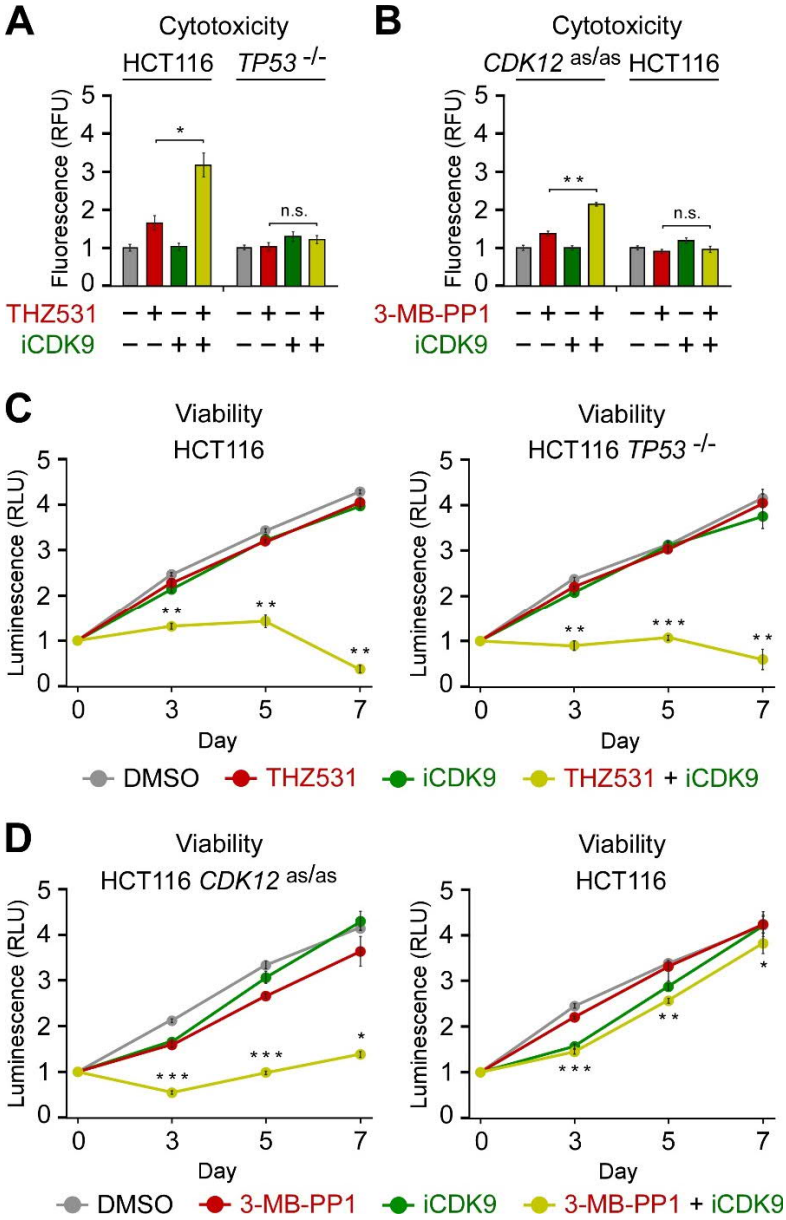

Supplementary Figure S3. Co-targeting of CDK12 and P-TEFb decreases viability of HCT116 cells.

(A,B) Cytotoxicity of HCT116 cell lines treated with DMSO, THZ531 (200 nM), 3-MB-PP1 (5 μM) and iCDK9 (25 nM) alone and in combination as indicated for 48 h measured using CellTox Green Cytotoxicity Assay. Results are presented as fluorescence values relative to the values of DMSO-treated cells and plotted as the mean ± s.e.m. (n = 3). *, P < 0.05; **, P < 0.01; n.s., non-significant, determined by Student's *t* test.

(C) Viability of HCT116 cell lines treated with DMSO, THZ531 (50 nM) and iCDK9 (25 nM) alone and in combination as indicated. Results obtained at the time points indicated below the graphs using CellTiter-Glo 2.0 Cell Viability Assay are presented as luminescence values relative to the values at Day 0 and plotted as the mean ± s.e.m. (n = 3). **, P < 0.01; ***, P < 0.001, determined by Student's *t* test using THZ531 and THZ531 + iCDK9 data sets.

(D) Viability of HCT116 cell lines treated with DMSO, 3-MB-PP1 (2.5 μM) and iCDK9 (5 nM) alone and in combination as indicated. Results obtained at the time points indicated below the graphs using CellTiter-Glo 2.0 Cell Viability Assay are presented as luminescence values relative to the values at Day 0 and plotted as the mean ± s.e.m. (n = 3). *, P < 0.05; **, P < 0.01, ***, P < 0.001, determined by Student's *t* test using 3-MB-PP1 and 3-MB-PP1 + iCDK9 data sets.

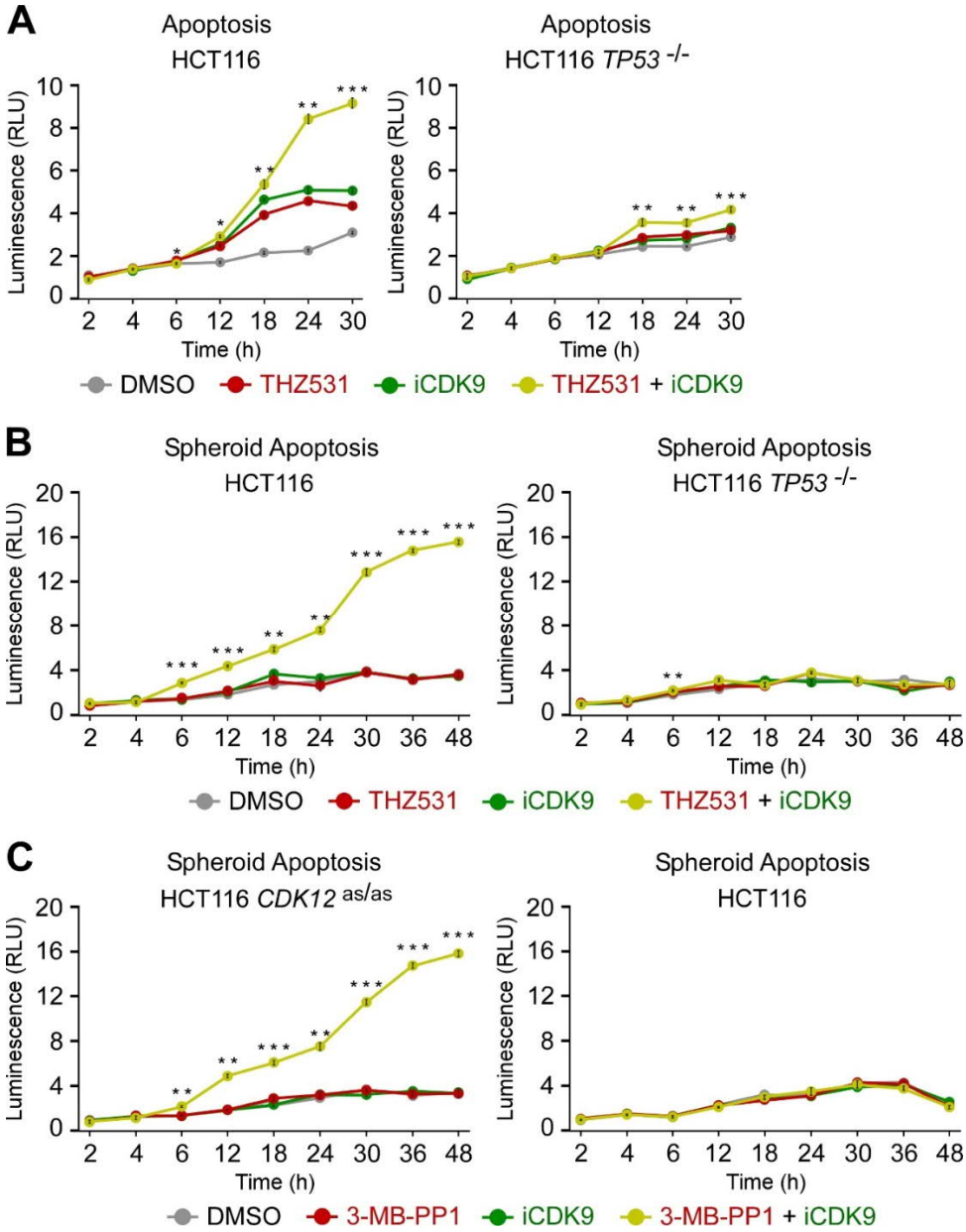

Supplementary Figure S4. Co-targeting of CDK12 and P-TEFb stimulates apoptosis of HCT116 cells.

(A) Apoptosis of HCT116 cell lines treated with DMSO, THZ531 (100 nM) and iCDK9 (25 nM) alone and in combination as indicated. Results obtained at the time points indicated below the graphs using RealTime-Glo Annexin V Apoptosis and Necrosis Assay are presented as luminescence values relative to the values of DMSO-treated cells at 2 h and plotted as the mean ± s.e.m. (n = 3). *, $P < 0.05$; **, $P < 0.01$; ***, $P < 0.001$, determined by Student's *t* test using THZ531 and THZ531 + iCDK9 data sets.

(B,C) Apoptosis of HCT116 cell line spheroid cultures treated with DMSO, THZ531 (100 nM), 3-MB-PP1 (5 μM) and iCDK9 (25 nM) alone and in combination as indicated. Spheroids were formed for 48 h prior to the treatments. Results obtained at the time points indicated below the graphs using RealTime-Glo Annexin V Apoptosis and Necrosis Assay are presented as luminescence values relative to the values of DMSO-treated cells at 2 h and plotted as the mean ± s.e.m. (n = 3). **, $P < 0.01$; ***, $P < 0.001$, determined by Student's *t* test using THZ531 and THZ531 + iCDK9 (B), and 3-MB-PP1 and 3-MB-PP1 + iCDK9 (C) data sets.

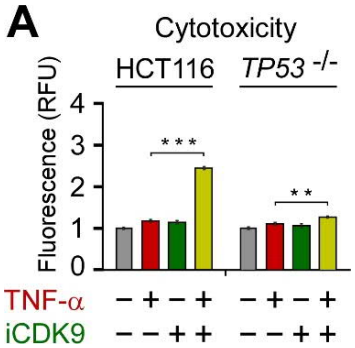

Supplementary Figure S5. Inhibition of CDK12 renders cancer cells dependent on the NF-κB signaling pathway.

(A) Cytotoxicity of HCT116 cell lines treated with DMSO, TNF-α (20 ng/ml) and iCDK9 (25 nM) alone and in combination as indicated for 48 h measured using CellTox Green Cytotoxicity Assay. Results are presented as fluorescence values relative to the values of DMSO-treated cells and plotted as the mean ± s.e.m. (n = 3). **, P < 0.01; ***, P < 0.001, determined by Student's *t* test.

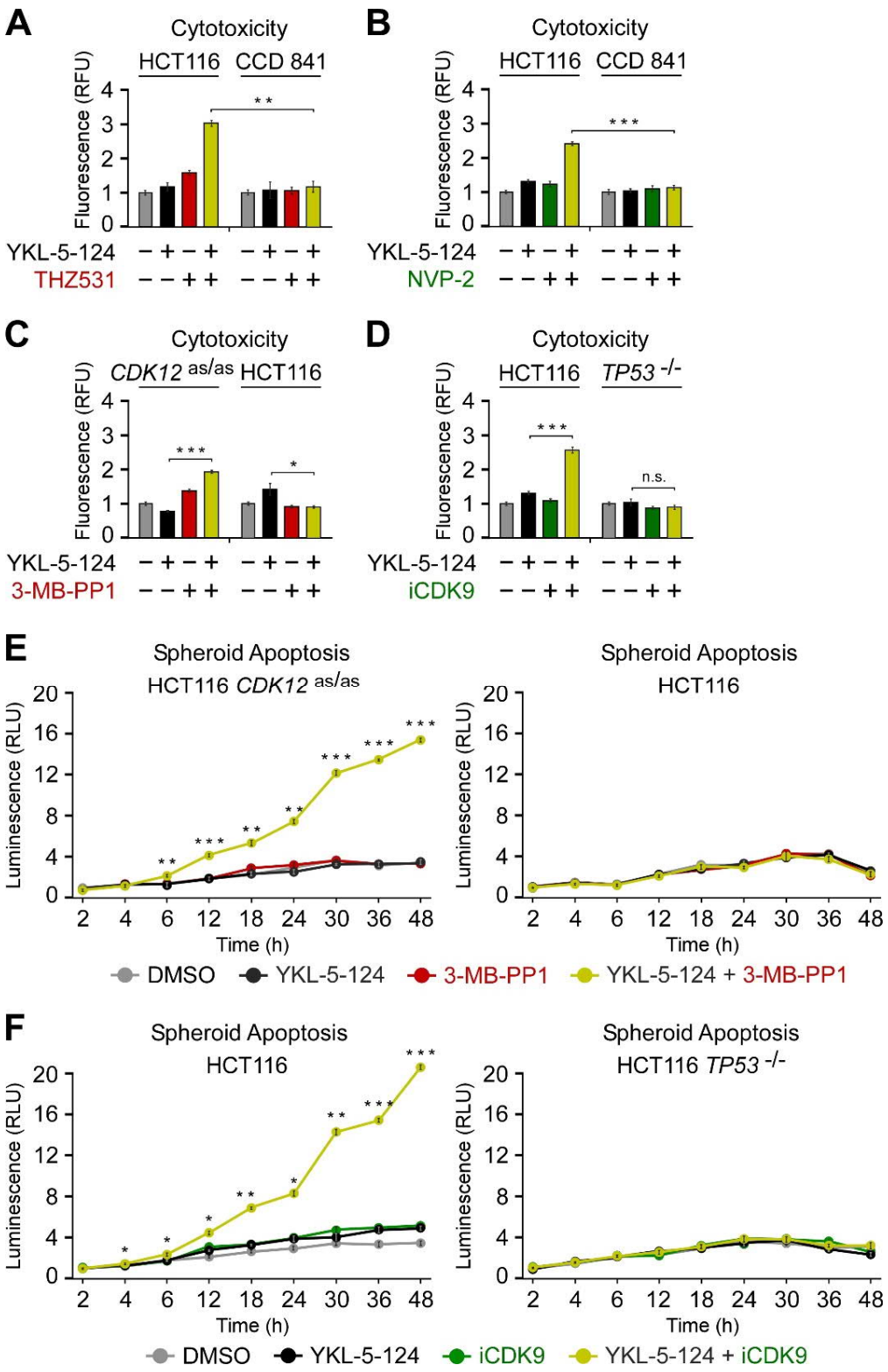

Supplementary Figure S6. Co-targeting of CDK7 and CDK12 or P-TEFb stimulates apoptosis of HCT116 cells.

(A-D) Cytotoxicity of the indicated cell lines treated with DMSO, YKL-5-124 (100 nM), THZ531 (200 nM), 3-MB-PP1 (5 μM), NVP-2 (10 nM) and iCDK9 (25 nM) alone and in combination as indicated for 48 h measured using CellTox Green Cytotoxicity Assay. Results are presented as fluorescence values relative to the values of DMSO-treated cells and plotted as the mean ± s.e.m. (n = 3). **, P < 0.01; ***, P < 0.001; n.s., non-significant, determined by Student's *t* test.

(E,F) Apoptosis of HCT116 cell line spheroid cultures treated with DMSO, YKL-5-124 (100 nM), 3-MB-PP1 (5 μM) and iCDK9 (25 nM) alone and in combination as indicated. Spheroids were formed for 48 h prior to the treatments. Results obtained at the time points indicated below the graphs using RealTime-Glo Annexin V Apoptosis and Necrosis Assay are presented as luminescence values relative to the values of DMSO-treated cells at 2 h and plotted as the mean ± s.e.m. (n = 3). *, $P < 0.05$; **, $P < 0.01$; ***, $P < 0.001$, determined by Student's *t* test using YKL-5-124 and YKL-5-124 + 3-MB-PP1 (F), and YKL-5-124 and YKL-5-124 + iCDK9 (F) data sets.

Supplementary Table S1A. Antibodies used in the study.

Antibody	Source	Identifier
Mouse monoclonal anti-CDK9	Santa Cruz Biotechnology	Cat#sc-13130; RRID: AB_627245
Mouse monoclonal anti-p53	Santa Cruz Biotechnology	Cat#sc-126; RRID: AB_628082
Mouse monoclonal anti-p21	Santa Cruz Biotechnology	Cat#sc-53870; RRID: AB_785026
Mouse monoclonal anti-GAPDH	Santa Cruz Biotechnology	Cat#sc-32233; RRID: AB_627679
Rabbit polyclonal anti-CDK12	Cell Signaling Technology	Cat#11973S; RRID: AB_2715688
Goat polyclonal anti-HEXIM1	Everest Biotech	Cat#EB06964; RRID: AB_2118260
Mouse monoclonal anti-CDK7	Cell Signaling Technology	Cat#2916; RRID: AB_2077142

Supplementary Table S1B. Chemicals used in the study.

Chemical	Source	Identifier
NVP-2	MedChemExpress	Cat#HY-12214A
i-CDK9	Qiang Zhou Laboratory (UC Berkeley)	N/A
THZ531	MedChemExpress	Cat#HY-103618
THZ532	Nathanael S. Gray Laboratory (Stanford University)	N/A
3-MB-PP1	Cayman Chemical	Cat#CAY17860
YKL-5-124	Nathanael S. Gray Laboratory (Stanford University)	N/A
TNF-α	Proteintech	Cat#HZ-1014
KU-60019	Selleck Chemicals	Cat#S1570
MLN120B	MedChemExpress	Cat#HY-15473
Triton X-100	Merck	Cat#108603
Propidium iodide	Merck	Cat#537059
RNase A	Thermo Fisher Scientific	Cat#12091021
EDTA-free Protease Inhibitor Cocktail	Merck	Cat#11873580001
Complete Protease Inhibitor Cocktail	Merck	Cat# 11697498001
PhosSTOP Phosphatase Inhibitor Cocktail	Merck	Cat# 4906837001
Phenylmethanesulfonyl fluoride	Merck	Cat# 10837091001
Random hexamers	Thermo Fisher Scientific	Cat#N8080127
TRI Reagent	Merck	Cat#T9424

Supplementary Table S1C. Commercial assays used in the study.

Assay	Source	Identifier
CellTox™ Green Cytotoxicity Assay	Promega	Cat#G8731
CellTiter-Glo® 2.0 Cell Viability Assay	Promega	Cat#G242
RealTime-Glo Annexin V Apoptosis and Necrosis Assay	Promega	Cat#JA1011
NP-40 lysis buffer	Thermo Fisher Scientific	Cat#J60766-AP
M-MLV reverse transcriptase	Thermo Fisher Scientific	Cat#28025-013
Turbo DNA-freeTM kit	Thermo Fisher Scientific	Cat#AM1907
Dynabeads Protein G	Thermo Fisher Scientific	Cat#10004D
FastStart Universal SYBR Green QPCR Master (Rox)	Merck	Cat#4913914001
Mycoplasmacheck detection kit	Eurofins	Cat#50400400

Supplementary Table S1D. Cell lines used in the study.

Cell line	Source	Identifier
HCT116 and HCT116 *TP53* $^{-/-}$	Joaquin M. Espinosa Laboratory (University of Colorado)	N/A
HCT116 and HCT116 *CDK12* $^{as/as}$	Dalibor Blazek Laboratory (CEITEC)	N/A
CCD 841 CoN	ATCC	Cat#CRL-1790

Supplementary Table S1E. Software and algorithms used in the study.

Software	Source	Identifier
R	N/A	https://www.R-project.org/
Molecular Signatures Database v6.0	GSEA - Broad Institute (Subramanian et al., 2005)	http://software.broadinstitute.org/gsea/msigdb/index.jsp

Supplementary Table S1F. DNA oligonucleotides used in RT-qPCR assay.

Gene	Primer Sequence (5'-3')
FOS	GAGGGAGCTGACTGATACA
	GAGGGATAAAGGAAAGCATAAGA
CDKN1A	TCTGCCTCCCAGAGTATTAG
	GAGTCCTGTGCTGTATTG
GAPDH	CGACCACTTTGTCAAGCTCA
	AGGGGAGATTCAGTGTGGTG

Supplementary Table 2A. GSEA of the differentially expressed genes of HCT116 *CDK12* $^{as/as}$ cells treated with 3-MB-PP1.

NAME	SIZE	NES	NOM p-val	FDR q-val
HALLMARK_TNFA_SIGNALING_VIA_NFKB	154	4.569116	0	0
HALLMARK_P53_PATHWAY	164	3.5234451	0	0
HALLMARK_UV_RESPONSE_UP	127	3.2683895	0	0
HALLMARK_HYPOXIA	137	3.1944003	0	0
HALLMARK_MYC_TARGETS_V1	195	3.0153737	0	0
HALLMARK_OXIDATIVE_PHOSPHORYLATION	177	2.8434043	0	0
HALLMARK_APOPTOSIS	120	2.4401872	0	0.001591778
HALLMARK_HEME_METABOLISM	140	2.336764	0	0.003460514
HALLMARK_IL2_STAT5_SIGNALING	129	2.177467	0	0.005861011
HALLMARK_ESTROGEN_RESPONSE_EARLY	156	2.0898244	0.002061856	0.009845811
HALLMARK_ESTROGEN_RESPONSE_LATE	149	1.9593471	0.007590133	0.024241297
HALLMARK_MTORC1_SIGNALING	178	1.8971316	0.014141414	0.031296957
HALLMARK_COMPLEMENT	107	1.8774587	0.004140787	0.032199197
HALLMARK_COAGULATION	59	1.8285226	0.018	0.037713073
HALLMARK_UNFOLDED_PROTEIN_RESPONSE	106	1.7999232	0.020618556	0.04069139
HALLMARK_TGF_BETA_SIGNALING	49	1.6993119	0.033195022	0.06621411
HALLMARK_CHOLESTEROL_HOMEOSTASIS	64	1.6154578	0.044	0.09267208
HALLMARK_WNT_BETA_CATENIN_SIGNALING	32	1.6126336	0.050632913	0.088545516
HALLMARK_FATTY_ACID_METABOLISM	114	1.5988237	0.049701788	0.08841487
HALLMARK_ANDROGEN_RESPONSE	82	1.5794183	0.048780486	0.09148346
HALLMARK_REACTIVE_OXYGEN_SPECIES_PATHWAY	40	1.5232025	0.043137256	0.11202551
HALLMARK_GLYCOLYSIS	164	1.448632	0.07465619	0.14750552
HALLMARK_UV_RESPONSE_DN	113	1.43242	0.08413002	0.1518739
HALLMARK_NOTCH_SIGNALING	28	1.4258226	0.10778443	0.14963925
HALLMARK_KRAS_SIGNALING_UP	93	1.4001325	0.10331384	0.15927574
HALLMARK_ALLOGRAFT_REJECTION	76	1.3723435	0.11173184	0.1728041
HALLMARK_ADIPOGENESIS	159	1.3482533	0.13800424	0.18155532
HALLMARK_INTERFERON_GAMMA_RESPONSE	113	1.2920843	0.17029703	0.21718231
HALLMARK_INFLAMMATORY_RESPONSE	88	1.2669091	0.20537429	0.23057935
HALLMARK_IL6_JAK_STAT3_SIGNALING	43	1.2235692	0.19832985	0.25934365
HALLMARK_ANGIOGENESIS	19	1.209937	0.22222222	0.26469308
HALLMARK_HEDGEHOG_SIGNALING	21	1.1713175	0.2631579	0.2921101
HALLMARK_PEROXISOME	81	1.0564362	0.35203093	0.41466853
HALLMARK_XENOBIOTIC_METABOLISM	116	1.0086775	0.4108818	0.46509293
HALLMARK_EPITHELIAL_MESENCHYMAL_TRANSITION	97	0.9805014	0.43128964	0.48777136
HALLMARK_MYOGENESIS	98	0.8351676	0.66539925	0.68373674
HALLMARK_APICAL_SURFACE	22	0.74281454	0.7335984	0.7931997

Supplementary Table 2B. GSEA of the metabolically-labeled transcriptome of IMR-32 cells treated with THZ531.

NAME	SIZE	NES	NOM p-val	FDR q-val
HALLMARK_MYC_TARGETS_V1	193	5.563506	0	0
HALLMARK_OXIDATIVE_PHOSPHORYLATION	177	5.0663924	0	0
HALLMARK_TNFA_SIGNALING_VIA_NFKB	99	4.719935	0	0
HALLMARK_UV_RESPONSE_UP	112	4.197955	0	0
HALLMARK_P53_PATHWAY	125	3.3015583	0	0
HALLMARK_MTORC1_SIGNALING	183	3.092014	0	0
HALLMARK_DNA_REPAIR	135	3.0866828	0	0
HALLMARK_HYPOXIA	127	2.9120805	0	0
HALLMARK_XENOBIOTIC_METABOLISM	95	2.8804173	0	0
HALLMARK_APOPTOSIS	98	2.8326726	0	0
HALLMARK_UNFOLDED_PROTEIN_RESPONSE	102	2.5896707	0	2.99E-04
HALLMARK_REACTIVE_OXYGEN_SPECIES_PATHWAY	40	2.549103	0	4.76E-04
HALLMARK_FATTY_ACID_METABOLISM	108	2.5357153	0.002024292	4.39E-04
HALLMARK_ADIPOGENESIS	147	2.5286474	0	4.08E-04
HALLMARK_MYC_TARGETS_V2	54	2.3626895	0	0.00146277
HALLMARK_PANCREAS_BETA_CELLS	15	2.232777	0.001923077	0.003968566
HALLMARK_PEROXISOME	74	2.171232	0.001996008	0.005409245
HALLMARK_E2F_TARGETS	195	2.1331124	0.001960784	0.00593865
HALLMARK_MYOGENESIS	79	2.0512328	0.007874016	0.008701
HALLMARK_GLYCOLYSIS	140	1.9735106	0.004	0.013776437
HALLMARK_INTERFERON_GAMMA_RESPONSE	79	1.9194916	0.015209125	0.017592223
HALLMARK_EPITHELIAL_MESENCHYMAL_TRANSITION	92	1.8656666	0.011976048	0.023216793
HALLMARK_G2M_CHECKPOINT	185	1.855756	0.00952381	0.023416903
HALLMARK_ESTROGEN_RESPONSE_LATE	109	1.8553507	0.015122874	0.0226012
HALLMARK_COAGULATION	39	1.844479	0.015686275	0.023018748
HALLMARK_ALLOGRAFT_REJECTION	59	1.76368	0.019417476	0.03456152
HALLMARK_APICAL_JUNCTION	94	1.7442787	0.02	0.036381908
HALLMARK_COMPLEMENT	92	1.7105255	0.025917927	0.041899767
HALLMARK_KRAS_SIGNALING_UP	72	1.6993793	0.03168317	0.04257905
HALLMARK_CHOLESTEROL_HOMEOSTASIS	57	1.6798801	0.04474708	0.04570205
HALLMARK_IL6_JAK_STAT3_SIGNALING	30	1.5345051	0.068359375	0.08708852
HALLMARK_NOTCH_SIGNALING	20	1.5226976	0.052941177	0.08898578
HALLMARK_ESTROGEN_RESPONSE_EARLY	109	1.4888661	0.09259259	0.10064545
HALLMARK_PI3K_AKT_MTOR_SIGNALING	80	1.3742985	0.1254902	0.16319123
HALLMARK_BILE_ACID_METABOLISM	52	1.3338807	0.13229571	0.1839347
HALLMARK_WNT_BETA_CATENIN_SIGNALING	27	1.2687906	0.1743487	0.23063491
HALLMARK_ANDROGEN_RESPONSE	76	1.2359577	0.21869159	0.2526209
HALLMARK_HEME_METABOLISM	125	1.2334836	0.1987705	0.2480089
HALLMARK_IL2_STAT5_SIGNALING	103	1.2308427	0.21399178	0.24436803
HALLMARK_INTERFERON_ALPHA_RESPONSE	35	1.1718471	0.2637131	0.2934957
HALLMARK_TGF_BETA_SIGNALING	43	1.169077	0.24950495	0.2889714

HALLMARK_KRAS_SIGNALING_DN	45	1.1259705	0.30737704	0.3246291
HALLMARK_SPERMATOGENESIS	66	1.1041087	0.32629558	0.341718
HALLMARK_INFLAMMATORY_RESPONSE	50	1.0801312	0.35546038	0.35893694
HALLMARK_ANGIOGENESIS	15	0.8187178	0.6785714	0.70232785
HALLMARK_HEDGEHOG_SIGNALING	26	0.68658835	0.87090164	0.8625199

Supplementary Table 2C. GSEA of the metabolically-labeled transcriptome of HeLa cells treated with 4-NQO.

NAME	SIZE	NES	NOM p-val	FDR q-val
HALLMARK_TNFA_SIGNALING_VIA_NFKB	183	2.4305887	0	0
HALLMARK_UV_RESPONSE_UP	137	2.065306	0	0
HALLMARK_P53_PATHWAY	186	1.988352	0	7.47E-04
HALLMARK_HYPOXIA	178	1.896474	0	0.001501905
HALLMARK_MYC_TARGETS_V1	197	1.8133836	0	0.003840972
HALLMARK_IL6_JAK_STAT3_SIGNALING	59	1.7889881	0.001727116	0.003999466
HALLMARK_KRAS_SIGNALING_UP	129	1.684865	0	0.007431363
HALLMARK_COAGULATION	101	1.6638521	0.001739131	0.008024147
HALLMARK_KRAS_SIGNALING_DN	112	1.6448113	0.001650165	0.009427669
HALLMARK_OXIDATIVE_PHOSPHORYLATION	196	1.6149383	0	0.012545925
HALLMARK_APOPTOSIS	140	1.6000311	0	0.013155066
HALLMARK_INFLAMMATORY_RESPONSE	136	1.5640745	0.003514939	0.018350631
HALLMARK_ALLOGRAFT_REJECTION	129	1.5362414	0.008237232	0.022455653
HALLMARK_XENOBIOTIC_METABOLISM	158	1.5266744	0.004918033	0.02225923
HALLMARK_DNA_REPAIR	141	1.5185546	0.006745363	0.02204756
HALLMARK_EPITHELIAL_MESENCHYMAL_TRANSITION	150	1.4969453	0.007961784	0.025071621
HALLMARK_UNFOLDED_PROTEIN_RESPONSE	109	1.4057269	0.039115645	0.05484522
HALLMARK_INTERFERON_GAMMA_RESPONSE	154	1.3858045	0.019672131	0.061199825
HALLMARK_COMPLEMENT	149	1.3687644	0.019169329	0.06666783
HALLMARK_IL2_STAT5_SIGNALING	152	1.3678787	0.027419355	0.06364318
HALLMARK_MTORC1_SIGNALING	194	1.3521531	0.022328548	0.06945896
HALLMARK_CHOLESTEROL_HOMEOSTASIS	68	1.3374736	0.07978723	0.075074576
HALLMARK_SPERMATOGENESIS	85	1.196419	0.16610739	0.20587933
HALLMARK_GLYCOLYSIS	182	1.0874748	0.26550078	0.39837846
HALLMARK_ESTROGEN_RESPONSE_LATE	160	1.0112025	0.42319748	0.5706809
HALLMARK_BILE_ACID_METABOLISM	85	0.97731715	0.49916527	0.6396823
HALLMARK_INTERFERON_ALPHA_RESPONSE	81	0.9755842	0.5042445	0.62018234
HALLMARK_MYOGENESIS	149	0.88848627	0.71756977	0.8318689
HALLMARK_FATTY_ACID_METABOLISM	136	0.8798573	0.7224026	0.82588035
HALLMARK_APICAL_JUNCTION	157	0.87212425	0.78110236	0.8163327
HALLMARK_MYC_TARGETS_V2	58	0.7980422	0.8500882	0.93908715
HALLMARK_TGF_BETA_SIGNALING	53	0.7200869	0.9259259	0.9893454
HALLMARK_E2F_TARGETS	198	0.7101401	0.99520767	0.96426207